

# A nonlinear multigrid for imaging electrical conductivity and permittivity at low frequency

**Liliana Borcea**

Computational and Applied Mathematics, MS 134, Rice University, 6100 Main Street, Houston, TX 77005-1892, USA

E-mail: borcea@caam.rice.edu

Received 23 May 2000, in final form 14 December 2000

## Abstract

We propose a nonlinear multigrid approach for imaging the electrical conductivity and permittivity of a body  $\Omega$ , given partial, usually noisy knowledge of the Neumann-to-Dirichlet map at the boundary. The algorithm is a nested iteration, where the image is constructed on a sequence of grids in  $\Omega$ , starting from the coarsest grid and advancing towards the finest one. We show various numerical examples that demonstrate the effectiveness and robustness of the algorithm and prove local convergence.

(Some figures in this article are in colour only in the electronic version; see [www.iop.org](http://www.iop.org))

## 1. Introduction

We consider the inverse problem of imaging electrical properties of a heterogeneous, isotropic material, in a domain  $\Omega$ , given low-frequency, alternating currents and voltages at the boundary  $\partial\Omega$ . The electrical properties of the material are described by the complex conductivity, or admittivity function

$$\rho(\mathbf{x}, \omega) = \sigma(\mathbf{x}) + i\omega\varepsilon(\mathbf{x}), \quad (1.1)$$

where  $\sigma(\mathbf{x})$  and  $\varepsilon(\mathbf{x})$  are the electrical conductivity and permittivity, and  $\omega$  is the frequency. The inverse problem, commonly referred to as *electrical impedance tomography*, has various applications in fields such as medical imaging [10], underground contaminant detection [38], subsurface flow monitoring [37], nondestructive testing [39], etc.

When all possible boundary currents and voltages are known, we have the Neumann-to-Dirichlet (NtD) map. In theory, given perfect data (full knowledge of the NtD map), the inverse problem has a unique answer over some large classes of functions  $\rho$  [7, 17, 20, 26, 30, 34, 44]. In practice, however, one never has the full NtD map and inversion is to be done with incomplete, noisy data. Furthermore, the inverse problem is ill posed [2], so some regularization strategy is needed to stabilize imaging techniques [3, 11, 14, 15, 18].

The numerical solution of the electrical impedance tomography problem has received increasing attention in the last decade and many imaging algorithms have been proposed,

especially for the static ( $\omega = 0$ ), dc case, where the unknown is  $\sigma$ , the electrical conductivity. There are basically three classes of algorithms:

- (1) Noniterative, linearization (Born approximation) algorithms which assume that  $\rho$  has small variations about a known admittivity function [2, 8, 9, 21].
- (2) Iterative, Newton-type imaging algorithms, based on either output least-squares [10, 14, 16, 46] or equation-error formulations [29, 45].
- (3) Layer stripping algorithms [12, 41, 43] which calculate  $\rho$  starting from the boundary and advancing in the interior of  $\Omega$ .

A very recent and promising algorithm has been developed by Nachman [34] and [40]. Finally, there are statistical, Bayesian approaches, where one can regularize the inverse problem by incorporating prior knowledge of the solution [28]. In spite of the rich literature on electrical impedance tomography, there are important, outstanding questions that do not have satisfactory answers, so far. For example, layer stripping algorithms are unstable and cannot be used for noisy data. The resolution and reliability of images of  $\rho$  have yet to be improved. The inversion algorithms have to be faster so images of  $\rho$  can be produced in real time. Finally, there are important issues to be resolved in experiment design and accuracy of the data [10].

In this paper, we propose a nonlinear multigrid approach [4, 5, 24] for the solution of the electrical impedance tomography problem. We formulate the numerical algorithm, prove local convergence and demonstrate its effectiveness through various numerical results. The formulation of the inverse problem is regularized, output least squares, where we minimize over admittivities  $\rho$  in an admissible set, the misfit in the voltage at the boundary. The nonlinear equation that we solve with the multigrid is the first-order optimality condition that the least-squares solution  $\rho$  must satisfy.

Suppose that we have a sequence of grids that discretize  $\Omega$ . Our inversion algorithm is a nested iteration [24] which constructs images of the admittivity, sequentially, starting from the coarsest grid and advancing towards the finest one. We emphasize that the algorithm is applied directly to the nonlinear problem, without any need of repeated linearization (see e.g. [4, 24] for a similar statement). Most computations are done on the coarse grid, where the nonlinear equation is solved with Newton's method. On finer grids, we do a few nonlinear relaxation iterations with the sole purpose of smoothing the error. Then, we update the solution through a coarse-grid correction. The algorithm that we propose can apply directly to any simply connected  $\Omega$  in  $\mathbb{R}^3$ . For simplicity, we do all our numerical calculations in a two-dimensional domain.

The main body of our algorithm can be found in classical multigrid literature [4, 5, 24]. However, to our knowledge, a nonlinear multigrid has not been applied in inversion, so far. Older results, such as [33], are limited to linearization (Born approximation), and use as data the Dirichlet-to-Neumann map, which seems more convenient in numerics. Nevertheless, in practice, due to noisy measurements, it is better to work with the NtD map, which is smoothing. We have found that, when using the NtD map in multigrid inversion, the coarse-grid computations need careful treatment, in order to get convergence, especially at the small regularization parameters we are interested in.

On the coarse grids, the numerical approximation of the electric potential  $\phi$  that solves the forward, Neumann boundary value problem can be quite inaccurate. For inversion, we compare  $\phi$  with the measured voltage, at the boundary. The inverse problem is ill posed, so we expect that the error in  $\phi$  is highly amplified in the coarse-grid image of  $\rho$ , unless we stabilize the inversion by choosing a large regularization parameter. Clearly, this is undesirable, because the images are too blurry. In this paper, we introduce an idea that allows us to perform inversion with small regularization parameters and therefore keep a good resolution of  $\rho$ , on

all grid levels. The idea amounts to taking a special projection of the excitation currents, on the coarse grid. To get this projection, we formulate an additional, coarse-grid, least-squares problem, which we solve once, at the beginning of the nested iteration. The computational cost of the coarse-grid solution is small and, as demonstrated by our numerical results, the coarse-grid images are often good approximations of the admittivity in  $\Omega$ . This is important in the multigrid iteration, for at least two reasons: good starting values in the nested iteration and effective coarse-grid corrections. The result is often a nice image on the fine grid, given at a low computational cost.

The paper is organized as follows: in section 2, we formulate the inverse problem and derive the nonlinear equation that is solved with the multigrid. In section 3, we describe the algorithm. In section 4, we introduce the ideas and numerical algorithm for coarse-grid imaging. In section 5, we present various numerical results that demonstrate the robustness and effectiveness of the nonlinear multigrid approach for the solution of the electrical impedance tomography problem. Finally, in section 6, we prove local convergence. Our proof is based on the known results in [24] and it assumes that the inverse problem is properly regularized.

## 2. Formulation of the problem

In this section, we give the regularized, output least-squares formulation of the inverse problem. The nonlinear equation that we solve with the multigrid is the first-order optimality condition that the least-squares solution must satisfy.

We consider a simply connected domain  $\Omega \subset \mathbb{R}^2$  containing an inhomogeneous, isotropic material with admittivity  $\rho(\mathbf{x}, \omega) = \sigma(\mathbf{x}) + i\omega\varepsilon(\mathbf{x})$ , satisfying

$$\begin{aligned} \text{real} [\rho(\mathbf{x})] &= \sigma(\mathbf{x}) \geq m_L > 0, \\ |\rho(\mathbf{x})| &= [\sigma^2(\mathbf{x}) + \omega^2\varepsilon^2(\mathbf{x})]^{\frac{1}{2}} \leq m_U, \end{aligned} \quad (2.1)$$

for all  $\mathbf{x} \in \Omega$  and some finite, positive constants  $m_L$  and  $m_U$ . Suppose that, at the boundary  $\partial\Omega$ , we apply a normal excitation current  $I(\mathbf{x}, \omega)$ . The electric potential  $\phi(\mathbf{x}, \omega)$  satisfies

$$\begin{aligned} \nabla \cdot [\rho(\mathbf{x}, \omega)\nabla\phi(\mathbf{x}, \omega)] &= 0 & \text{in } \Omega, \\ \rho(\mathbf{x}, \omega)\nabla\phi(\mathbf{x}, \omega) \cdot \mathbf{n}(\mathbf{x}) &= I(\mathbf{x}, \omega) & \text{on } \partial\Omega, \end{aligned} \quad (2.2)$$

where  $\mathbf{n}(\mathbf{x})$  is the outer normal to  $\partial\Omega$ . The Neumann boundary value problem (2.2) is derived from Maxwell's equations, in the limit of small  $\omega$ , as shown in [10]. We assume a fixed frequency and, to simplify notation, we henceforth drop  $\omega$  from the arguments of  $\rho$ ,  $\phi$  and  $I$ . It is well known (see e.g. [19]) that for current densities  $I(\mathbf{x})$  satisfying  $\int_{\partial\Omega} I(s) ds = 0$ , (2.2) has a solution  $\phi(\mathbf{x}) \in H^1(\Omega)$ , that is unique up to an additive constant. We fix this constant by

$$\int_{\partial\Omega} \phi(s) ds = \int_{\partial\Omega} V(s) ds, \quad (2.3)$$

where  $V$  is the measured potential at the boundary.

In the inverse problem,  $\rho(\mathbf{x})$  is unknown and it is to be found from simultaneous measurements of currents and potentials at the boundary. Thus, for a given  $I(\mathbf{x})$ , we overspecify (2.2) by requiring that, at the true admittivity function  $\rho(\mathbf{x})$ , the potential satisfy

$$\phi(\mathbf{x}) = V(\mathbf{x}) \quad \text{for } \mathbf{x} \in \partial\Omega. \quad (2.4)$$

When all possible excitations  $I(\mathbf{x})$  and measurements  $V(\mathbf{x})$  are available, we know the NtD map

$$\Lambda_\rho : H^{-\frac{1}{2}}(\partial\Omega) \rightarrow H^{\frac{1}{2}}(\partial\Omega), \quad \Lambda_\rho I(\mathbf{x}) = V(\mathbf{x}), \quad \text{for } \mathbf{x} \in \partial\Omega. \quad (2.5)$$

In practice, however, we only have partial knowledge about  $\Lambda_\rho$ . That is, we have a set of currents  $\{I_j(\mathbf{x})\}_{j=1}^{N_{\text{exp}}}$  and corresponding voltage measurements  $\{V_j(\mathbf{x}_p)\}_{j=1}^{N_{\text{exp}}}$ . Here, index  $j$  represents the experiment, or current excitation  $I(\mathbf{x}) = I_j(\mathbf{x})$  in (2.2), and  $\mathbf{x}_p \in \partial\Omega$ ,  $p = 1, \dots, N_B$ , denote points of measurement of the resulting potential  $V_j$  at the boundary.

The inverse problem is: find  $\rho(\mathbf{x})$  in the interior of  $\Omega$ , given boundary data  $\{I_j(\mathbf{x})\}_{j=1}^{N_{\text{exp}}}$  and  $\{V_j(\mathbf{x}_p)\}_{j=1}^{N_{\text{exp}}}$ , for  $p = 1, \dots, N_B$ . We consider the output least-squares formulation:

$$\text{Minimize over } \rho \in \Upsilon, \text{ functional } J(\rho) = \sum_{j=1}^{N_{\text{exp}}} \|R_j(\rho) - V_j\|_{L^2(\partial\Omega)}^2, \quad (2.6)$$

where we take some interpolation between the points of measurement of potential  $V_j$ . We are concerned with finding  $\rho$  in the interior of  $\Omega$  so we assume that we know the admittivity at the boundary. The set  $\Upsilon$  of admissible  $\rho$  is defined by

$$\Upsilon = \{\rho \in L^2(\Omega), \rho \text{ satisfies (2.1) and, at the boundary, } \rho(\mathbf{x}) = \tilde{\rho}(\mathbf{x}), \text{ given for } \mathbf{x} \in \partial\Omega\}. \quad (2.7)$$

In (2.6),  $R_j$  is the map

$$R_j : \Upsilon \rightarrow L^2(\partial\Omega), \quad R_j(\rho) = \Lambda_\rho I_j = \text{trace of } \phi_j \text{ at the boundary}, \quad (2.8)$$

where  $\phi_j$  is the solution of

$$\begin{aligned} \nabla \cdot [\rho(\mathbf{x}) \nabla \phi_j(\mathbf{x})] &= 0 & \text{in } \Omega, \\ \rho(\mathbf{x}) \nabla \phi_j(\mathbf{x}) \cdot \mathbf{n}(\mathbf{x}) &= I_j(\mathbf{x}) & \text{on } \partial\Omega, \\ \int_{\partial\Omega} \phi_j(s) \, ds &= \int_{\partial\Omega} V_j(s) \, ds. \end{aligned} \quad (2.9)$$

We have the following theoretical results.

**Lemma 1.**  $R_j(\rho)$  is a continuous map. That is, for an arbitrary perturbation  $\delta\rho$  such that  $\rho + \delta\rho \in \Upsilon$ , there exists a finite, positive constant  $c$  such that  $\|R_j(\rho + \delta\rho) - R_j(\rho)\|_{L^2(\partial\Omega)} \leq c \|\delta\rho\|_{L^\infty(\Omega)}$ . Moreover, if  $\rho, \delta\rho \in C^{k,1}(\bar{\Omega})$ , where  $\bar{\Omega}$  is the closure of  $\Omega$  and  $k$  is strictly positive, we have  $\|R_j(\rho + \delta\rho) - R_j(\rho)\|_{L^2(\partial\Omega)} \leq c \|\delta\rho\|_{L^2(\Omega)}$ .

**Lemma 2.**  $R_j(\rho)$  is Fréchet differentiable, with Fréchet derivative  $DR_j(\rho)\delta\rho = \delta\phi_j|_{\partial\Omega}$ , where  $\delta\phi_j$  solves the linearized problem

$$\begin{aligned} \nabla \cdot [\rho(\mathbf{x}) \nabla \delta\phi_j(\mathbf{x})] &= -\nabla \cdot [\delta\rho(\mathbf{x}) \nabla \phi_j(\mathbf{x})] & \text{in } \Omega, \\ \nabla \delta\phi_j(\mathbf{x}) \cdot \mathbf{n}(\mathbf{x}) &= 0 & \text{on } \partial\Omega, \\ \int_{\partial\Omega} \delta\phi_j(s) \, ds &= 0. \end{aligned} \quad (2.10)$$

Proofs of lemmas 1 and 2 are given in [14]. The Fréchet derivative operator defined in lemma 2 is compact (see e.g. [11]), and so problem (2.6) is ill posed.

We consider the regularization

$$\min_{\rho \in \Upsilon} J_\alpha(\rho), \quad \text{where } J_\alpha(\rho) = J(\rho) + \alpha \|\nabla \rho\|_{L^2(\Omega)}^2, \quad (2.11)$$

and  $\alpha > 0$  is a small regularization parameter.

**Lemma 3.** For all  $\alpha > 0$ , the functional  $J_\alpha$  has at least one minimizer  $\rho_\alpha$  in the set  $\Upsilon \cap H^1(\Omega)$ .

**Proof.** Choose a sequence  $\{\rho_i\} \in \Upsilon$  such that  $J_\alpha(\rho_i) \rightarrow J_\alpha^* = \inf\{J_\alpha(\rho), \text{ where } \rho \in \Upsilon\}$ . Due to the regularization term  $\alpha\|\nabla\rho\|_{L^2(\Omega)}^2$  in (2.11), for  $i$  sufficiently large, we have  $\rho_i \in H^1(\Omega)$ . Moreover,  $\rho_i(x) - \tilde{\rho}(x) \in H_0^1(\Omega)$ , where we take the harmonic extension, inside  $\Omega$ , of the known  $\tilde{\rho}$  at the boundary. The compact embedding  $H_0^1(\Omega) \subset\subset L^2(\Omega)$  [1] shows us that there is a subsequence, denoted by  $\{\rho_{i_k} - \tilde{\rho}\}$ , that converges to  $\rho_\alpha - \tilde{\rho}$ , strongly in  $L_2(\Omega)$ . Finally, lemma 1 implies that  $J_\alpha$  is a continuous functional in  $L_2(\Omega)$  so  $\rho_i \rightarrow \rho_\alpha$  means  $J_\alpha(\rho_i) \rightarrow J_\alpha(\rho_\alpha) = J_\alpha^*$ . Thus,  $\rho_\alpha \in \Upsilon \cap H^1(\Omega)$  is a minimizer of  $J_\alpha(\rho)$  and lemma 3 is proved.  $\square$

By taking the first variation of functional  $J_\alpha(\rho)$ , we find that, at a minimum,  $\rho(x)$  satisfies the first-order optimality condition

$$-\alpha\Delta\rho(x) + \sum_{j=1}^{N_{\text{exp}}} [DR_j(\rho)]^* [R_j(\rho) - V_j](x) = 0, \quad x \in \Omega, \quad (2.12)$$

where  $[DR_j(\rho)]^*$  is the  $L_2$  adjoint of the Fréchet derivative  $DR_j$  defined in lemma 2. Note that (2.12) is valid if the minimizer is in the interior of  $\Upsilon$ . Otherwise, one has additional terms in (2.12). For example, it may be necessary that the strict positivity of the real part of  $\rho$  be enforced, in which case one must add a penalty term in (2.11), by means of a Lagrange multiplier [23]. Such extra complications are not addressed in this paper, where we assume that our solution is in the interior of  $\Upsilon$  and we solve the nonlinear equation (2.12) with a multigrid approach. First, we observe that, in (2.12), terms involving the adjoint operators  $[DR_j(\rho)]^*$  can be written in more explicit form as shown in lemma 4.

**Lemma 4.** For any function  $\chi_j \in L^2(\partial\Omega)$ , such that  $\int_{\partial\Omega} \chi_j(s) ds = 0$ , we have

$$[DR_j(\rho)]^* \chi_j(x) = -\nabla\bar{\phi}_j(x) \cdot \nabla\psi_j(x), \quad (2.13)$$

where  $\bar{\phi}_j$  is the complex conjugate of  $\phi_j$ , the solution of (2.9), and  $\psi_j$  solves the adjoint equation

$$\begin{aligned} \nabla \cdot [\bar{\rho}(x)\nabla\psi_j(x)] &= 0 && \text{in } \Omega, \\ \bar{\rho}(x)\nabla\psi_j(x) \cdot \mathbf{n}(x) &= \chi_j(x) && \text{on } \partial\Omega, \\ \int_{\partial\Omega} \psi_j(s) ds &= 0. \end{aligned} \quad (2.14)$$

The proof of lemma 4 is similar to that given in [14,35] for the particular case of the real-valued function  $\rho$  in  $L^2(\Omega)$ . From (2.10) and (2.14), we have

$$\begin{aligned} \int_{\Omega} \{\delta\bar{\phi}_j(x)\nabla \cdot [\bar{\rho}(x)\nabla\psi_j(x)] - \psi_j(x)\nabla \cdot [\bar{\rho}(x)\nabla\delta\bar{\phi}_j(x)]\} dx \\ = \int_{\Omega} \psi_j(x)\nabla \cdot [\delta\bar{\rho}(x)\nabla\bar{\phi}_j(x)] dx, \end{aligned}$$

where the overbar indicates the complex conjugate. Integrating by parts and using lemma 2, we obtain

$$\begin{aligned} \int_{\partial\Omega} \{\delta\bar{\phi}_j(s)\bar{\rho}(s)\nabla\psi_j(s) \cdot \mathbf{n}(s) - \psi_j(s)\bar{\rho}(s)\nabla\delta\bar{\phi}_j(s) \cdot \mathbf{n}(s)\} ds \\ = \int_{\partial\Omega} [\overline{DR_j(\rho)\delta\rho}] \chi_j(s) ds = \int_{\Omega} \delta\bar{\rho}(x)[DR_j(\rho)]^* \chi_j(x) dx \\ = - \int_{\Omega} \delta\bar{\rho}(x)\nabla\bar{\phi}_j(x) \cdot \nabla\psi_j(x) dx. \end{aligned}$$

This holds for arbitrary perturbations  $\delta\rho$ , such that  $\rho + \delta\rho \in \Upsilon$  and (2.13) follows.

We use lemma 4 with  $\chi_j = R_j(\rho) - V_j$  and rewrite equation (2.12) as

$$-\alpha \Delta \rho(\mathbf{x}) - \sum_{j=1}^{N_{\text{exp}}} \nabla \bar{\phi}_j(\mathbf{x}; \rho) \cdot \nabla \psi_j(\mathbf{x}; \rho) = 0, \quad \mathbf{x} \in \Omega, \quad (2.15)$$

where we emphasize that  $\phi_j$  and  $\psi_j$  depend nonlinearly on the unknown admittivity function  $\rho$ . Moreover, equation (2.15) is coupled with equations (2.9) and (2.14), satisfied by potentials  $\phi_j$  and  $\psi_j$ , for each  $\rho$  and excitation  $I_j$ ,  $j = 1, \dots, N_{\text{exp}}$ . In what follows, we focus attention on the nonlinear multigrid numerical solution of (2.15).

### 3. Nonlinear multigrid solution

In this section, we describe the nonlinear multigrid algorithm for solving equation (2.15), with Dirichlet boundary conditions

$$\rho(\mathbf{x}) = \tilde{\rho}(\mathbf{x}) \quad \text{on } \partial\Omega. \quad (3.1)$$

We write (2.15) and (3.1) in abstract form

$$\mathcal{F}(\alpha, \rho) = 0, \quad (3.2)$$

where the unknown is  $\rho$  and  $\alpha$  is the regularization parameter.

#### 3.1. Discretization

In a multigrid approach, equation (3.2) is discretized on a sequence  $\{G_l\}_{l=0}^K$  of grids, where  $G_0$  is the coarsest grid, which we take with uniform spacing  $h_0$ . We define grid  $G_l$  as

$$G_l = \{(x_i, y_j) = (i h_l, j h_l) \in \mathbb{R}^2, i, j \in \mathbb{Z}\} \cap \text{interior } \Omega, \quad (3.3)$$

where  $h_l = \frac{h_0}{2^l}$ ,  $l = 0, 1, \dots, K$ .

Note that the uniform discretization (3.3) holds for the interior of  $\Omega$ . Depending on the shape of  $\Omega$ , near the boundary, the grid points may be irregular, such as  $(s h_l, t h_l)$ , where  $s$  and  $t$  may not be integers. We call the set of discrete boundary points  $\partial G_l$ , and define the set  $\bar{G}_l = G_l \cup \partial G_l$ , which contains all discretization points at level  $l$ , in  $\bar{\Omega}$ .

For simplicity, let us take a unit square domain  $\Omega$ , such that  $(x_i, y_j) = (i h_l, j h_l)$ , for  $i, j = 0, \dots, n_l$ , are the grid points of  $\bar{G}_l$ . The finite-difference discretization of (3.2) is

$$\mathcal{F}_l(\alpha_l, \rho^{(l)}) = \mathbf{0}, \quad (3.4)$$

where  $\alpha_l$  and  $\rho^{(l)}$  are the regularization parameter and the restriction of  $\rho$  on grid  $G_l$ , respectively. We use a nine-point, finite-difference scheme

$$\begin{aligned} [\mathcal{F}_l(\alpha_l, \rho^{(l)})]_{ij} = & -\frac{\alpha_l}{h_l^2} (\rho_{i+1,j+1}^{(l)} + \rho_{i-1,j+1}^{(l)} + \rho_{i+1,j-1}^{(l)} + \rho_{i-1,j-1}^{(l)} + 4\rho_{i+1,j}^{(l)} + 4\rho_{i-1,j}^{(l)} \\ & + 4\rho_{i,j+1}^{(l)} + 4\rho_{i,j-1}^{(l)} - 20\rho_{i,j}^{(l)}) - \sum_{k=1}^{N_{\text{exp}}} \left[ \left( \frac{\bar{\phi}_k(x_{i+1}, y_j) - \bar{\phi}_k(x_{i-1}, y_j)}{2h_l} \right) \right. \\ & \times \left( \frac{\psi_k(x_{i+1}, y_j) - \psi_k(x_{i-1}, y_j)}{2h_l} \right) \\ & \left. + \left( \frac{\bar{\phi}_k(x_i, y_{j+1}) - \bar{\phi}_k(x_i, y_{j-1})}{2h_l} \right) \left( \frac{\psi_k(x_i, y_{j+1}) - \psi_k(x_i, y_{j-1})}{2h_l} \right) \right] = 0, \quad (3.5) \end{aligned}$$

where  $\rho_{i,j}^{(l)} = \rho^{(l)}(x_i, y_j)$ , for all  $(x_i, y_j) \in G_l$ .

A numerical approximation of  $\phi_k(x_i, y_j)$  and  $\psi_k(x_i, y_j)$  is obtained by solving equations (2.9) and (2.14) with a piecewise linear, finite-element method (see e.g. [27]). Let  $\mathcal{T}_l$  be a triangulation of  $\Omega$  with vertices given by the grid points in  $G_l$ . In each triangle of  $\mathcal{T}_l$ , we take the admittivity  $\rho$  as a piecewise linear interpolation of the values of  $\rho^{(l)}$  at grid points  $(x_i, y_j) \in G_l$ . We define the vector of unknowns

$$\phi_j^{(l)} = \begin{pmatrix} \phi_j^{(l)}(\text{interior}) \\ \phi_j^{(l)}(\text{boundary}) \end{pmatrix} \in \mathbb{C}^{(n_l+1)^2}, \tag{3.6}$$

where  $\phi_j^{(l)}(\text{interior}) \in \mathbb{C}^{(n_l-1)^2}$  contains the values of  $\phi_j^{(l)}$  at the interior nodes and  $\phi_j^{(l)}(\text{boundary}) \in \mathbb{C}^{4n_l}$  is the vector of boundary potentials. The finite-element discretization of (2.9) leads to the linear system of equations

$$A^{(l)}(\rho^{(l)})\phi_j^{(l)} = \mathbf{b}^{(l)}(I_j), \tag{3.7}$$

where  $A^{(l)}$  is an  $(n_l + 1)^2 \times (n_l + 1)^2$ , complex matrix that depends linearly on  $\rho^{(l)}$  and  $\mathbf{b}^{(l)}$  is an  $(n_l + 1)^2$ -dimensional complex vector that depends linearly on the excitation current  $I_j$ . Due to the well-posedness of (2.9),  $A^{(l)}$  is invertible and the solution  $\phi_j^{(l)}$  exists and is unique. Similarly, the finite-element solution of (2.14) leads to

$$A^{(l)}(\overline{\rho^{(l)}})\Psi_j^{(l)} = \mathbf{c}^{(l)}(\rho^{(l)}), \tag{3.8}$$

where  $A^{(l)}$  is the same as in (3.7), except that it depends on the complex conjugate of  $\rho^{(l)}$ . Note that the right-hand side in (3.8) depends nonlinearly on  $\rho^{(l)}$ , due to the adjoint excitation current  $\chi_j = \phi_j - V_j$  defined at the boundary.

In the multigrid, one must transfer functions from one grid to the next. This is done through prolongation and restriction operators. For  $\rho^{(l)}$  and  $\rho^{(l-1)}$  given on grids  $G_l$  and  $G_{l-1}$ , we define the prolongation  $\mathcal{P}$  and restriction  $\mathcal{R}$  by

$$\begin{aligned} \rho^{(l)} &= \mathcal{P}\rho^{(l-1)}, \\ \rho^{(l-1)} &= \mathcal{R}\rho^{(l)}, \end{aligned} \quad l = 1, \dots, K. \tag{3.9}$$

Since our differential equation is of second order, it suffices to take  $\mathcal{P}$  as a piecewise linear interpolation [24]. We choose the nine-point prolongation  $\mathcal{P}$  and the full weighted restriction  $\mathcal{R}$ , which is the adjoint of  $\mathcal{P}$  [24].

We conclude with the observation that our finite-difference discretizations  $\mathcal{F}_{l-1}$  and  $\mathcal{F}_l$ , on adjacent grids  $G_{l-1}$  and  $G_l$ , are independent. In other words, we can seek a solution of (3.4) on  $G_{l-1}$ , independent of the fact that we actually wish to solve (3.4) on  $G_l, G_{l+1}, \dots, G_K$ . This is essential in a multigrid, where coarse-grid computations are needed to correct the solutions on the finer grids. Another possible discretization of (3.2) is given by the conforming finite-element (Galerkin) approach. Then,  $\mathcal{F}_{l-1}(\rho^{(l-1)}) = \mathcal{R}\mathcal{F}_l(\mathcal{P}\rho^{(l-1)})$ , as shown in [24]. This discretization has the advantage of a perfect *relative consistency* ( $\mathcal{F}_{l-1} - \mathcal{R}\mathcal{F}_l\mathcal{P} = 0$ ), which is important in coarse-grid correction [24]. However, the Galerkin approach has the major disadvantage that  $\mathcal{F}_{l-1}$  depends on  $\mathcal{F}_l$ . This means that the evaluation of  $\mathcal{F}_{l-1}$  and its Jacobian, on coarse grid  $G_{l-1}$ , requires the calculation of  $\mathcal{F}_l(\mathcal{P}\rho^{(l-1)})$  and its Jacobian, on the finer grid,  $G_l$ . This is clearly too expensive and leaves us with the only choice of a finite-difference discretization, such as (3.5).

### 3.2. The nonlinear multigrid algorithm

For numerical computations, we transform the complex problem (3.4) into a real system of equations, with real unknowns. We define

$$\mathbf{u}_l = \begin{pmatrix} \text{real } \rho_{1,1}^{(l)} \\ \text{real } \rho_{1,2}^{(l)} \\ \vdots \\ \text{real } \rho_{n_l-1,n_l-1}^{(l)} \\ \text{imag } \rho_{1,1}^{(l)} \\ \vdots \\ \text{imag } \rho_{n_l-1,n_l-1}^{(l)} \end{pmatrix} = \begin{pmatrix} \sigma_{1,1}^{(l)} \\ \sigma_{1,2}^{(l)} \\ \vdots \\ \sigma_{n_l-1,n_l-1}^{(l)} \\ \omega \varepsilon_{1,1}^{(l)} \\ \vdots \\ \omega \varepsilon_{n_l-1,n_l-1}^{(l)} \end{pmatrix} \in \mathbb{R}^{2(n_l-1)^2}, \quad (3.10)$$

and rewrite (3.4) as

$$\mathcal{L}_l(\mathbf{u}_l) = \begin{pmatrix} \text{real } [\mathcal{F}_l]_{1,1} \\ \vdots \\ \text{real } [\mathcal{F}_l]_{n_l-1,n_l-1} \\ \text{imag } [\mathcal{F}_l]_{1,1} \\ \vdots \\ \text{imag } [\mathcal{F}_l]_{n_l-1,n_l-1} \end{pmatrix} = \mathbf{0}. \quad (3.11)$$

To solve (3.11), starting with the coarsest grid  $G_0$  and advancing towards the finest grid  $G_K$ , we use the nonlinear *nested iteration* [24] algorithm sketched below:

- Choose  $\alpha_0$ .
- Calculate  $\mathbf{u}_0 \approx \mathcal{L}_0^{-1}(\mathbf{0})$ .
- For  $l = 1, \dots, K$ ,
  - $\mathbf{u}_l = \mathcal{P}\mathbf{u}_{l-1}$ . (3.12)
  - Choose  $\alpha_l$  and set  $\alpha_k = \alpha_l$ , for  $k = 0, 1, \dots, l-1$ .
  - call **NMGM**( $l, \mathbf{u}_l, \mathbf{0}$ )  $\tilde{M}$  times.
- End.

In (3.12),  $K$  and  $\tilde{M}$  are defined by the user. In our implementation, the index  $K$  of the finest grid is 2 and  $\tilde{M} = 3$ . On the coarsest grid  $G_0$ , we solve  $\mathcal{L}_0(\mathbf{u}_0) = \mathbf{0}$  with Newton's method [13]. The initial guess of  $\rho^{(0)}$  or, equivalently,  $\mathbf{u}_0$ , is the restriction on  $G_0$  of the harmonic extension in  $\Omega$ , of the known  $\tilde{\rho}$  at  $\partial\Omega$ .

Procedure **NMGM** ( $l, \mathbf{u}_l, \mathbf{g}_l$ ) performs the nonlinear multigrid iteration for solving

$$\mathcal{L}_l(\mathbf{u}_l) = \mathbf{g}_l. \quad (3.13)$$

The important elements of **NMGM** are a *smoothing* or *relaxation* process and a *coarse-grid correction*. The purpose of smoothing on grid  $G_l$  is not to solve (3.13), but rather to reduce the high-frequency components in the error  $\mathbf{u}_l - \mathcal{L}_l^{-1}(\mathbf{g}_l)$ . This allows us to approximate the error on the coarse grid  $G_{l-1}$ , where solution is cheaper. Finally, given the coarse-grid solution, we update  $\mathbf{u}_l$  on  $G_l$ , through the coarse-grid correction.

Let us describe the smoothing (relaxation) process denoted by

$$\mathbf{u}_l \leftarrow \mathcal{S}_l^{(v)}(\mathbf{u}_l, \mathbf{g}_l), \quad (3.14)$$

where index  $v$  stands for the number of relaxation sweeps. We choose a block nonlinear Gauss–Seidel smoother, where the blocks of unknowns are defined as follows: consider a grid point  $(x_i, y_j) \in G_l$  and define the set  $\mathcal{N}_{ij} = \{(x_k, y_p) \in G_l \text{ such that } |k - i| \leq 1 \text{ and } |p - j| \leq 1\}$ .

Note that  $\mathcal{N}_{ij}$  is the set of closest neighbours of  $(x_i, y_j)$ , in the interior of  $\Omega$ . Moreover,  $\mathcal{N}_{ij}$  contains the grid points of the nine-point stencil of discretization (3.5). A block of unknowns in our Gauss–Seidel scheme consists of the components of  $\mathbf{u}_l$  that correspond to  $\sigma^{(l)}(\mathbf{x})$  and  $\omega\varepsilon^{(l)}(\mathbf{x})$ , at points  $\mathbf{x} \in \mathcal{N}_{ij}$ . Let us denote by  $\mathcal{I}_m$  the set of indices of components of  $\mathbf{u}_l$  that belong to such a block, and suppose that we have a total of  $M_l$  blocks. The nonlinear Gauss–Seidel relaxation scheme is

$$\begin{aligned} &\text{For } m = 1, \dots, M_l, \\ &\quad \mathbf{u}_{l,r} = \mathbf{u}'_{l,r}, \quad \text{for all } r \in \mathcal{I}_m, \\ &\quad \text{where } \mathbf{u}'_{l,r} \text{ are solutions of the nonlinear system of equations} \quad (3.15) \\ &\quad \mathcal{L}_{l,r}(\{\mathbf{u}_{l,p}, p \notin \mathcal{I}_m\}, \{\mathbf{u}'_{l,p}, p \in \mathcal{I}_m\}) = \mathbf{g}_{l,r}, \quad r \in \mathcal{I}_m. \\ &\text{End.} \end{aligned}$$

In [4, 24], it is shown that it is not necessary to solve the nonlinear system of equations in (3.15). Instead, we just take one Newton step toward its solution. As emphasized in [4], this is not related to any global linearization of our problem. We just linearize a few equations in (3.13), with respect to a few unknowns, for the sole purpose of smoothing the error. At small  $\alpha_l$ , making a full Newton step might not be satisfactory [13]. Instead, we use a line search approach, where we take a fraction  $\lambda_m$  of the Newton step. The line search parameter  $\lambda_m$  is calculated such that the sum of square residuals at grid points  $\mathbf{x} \in G_l$ , satisfying  $|\mathbf{x} - (x_i, y_j)| \leq kh_l$ , does not increase after updating  $\mathbf{u}'_{l,p}$ , for all  $p \in \mathcal{I}_m$ . In our numerical experiments, we take  $k = 3$ .

We have implemented two versions of procedure **NMGM**. The first version is the *full approximation storage* (FAS) algorithm introduced in [5].

$$\begin{aligned} &\text{Procedure } \mathbf{NMGM}(l, \mathbf{u}_l, \mathbf{g}_l) : \\ &\text{If } l = 0, \\ &\quad \mathbf{u}_l = \mathcal{L}_0^{-1}(\mathbf{g}_l). \\ &\text{Else,} \\ &\quad \text{do } \nu_1 \text{ pre-smoothing iterations } \mathbf{u}_l \leftarrow \mathcal{S}_l^{(\nu_1)}(\mathbf{u}_l, \mathbf{g}_l). \\ &\quad \mathbf{v} = \mathcal{R}\mathbf{u}_l, \\ &\quad \mathbf{d} = \mathcal{L}_{l-1}(\mathbf{v}) + \mathcal{R}[\mathbf{g}_l - \mathcal{L}_l(\mathbf{u}_l)], \\ &\quad \mathbf{w} = \mathbf{v}. \\ &\quad \text{Call } \mathbf{NMGM}(l-1, \mathbf{w}, \mathbf{d}) \text{ } M \geq 2 \text{ times.} \\ &\quad \text{Do coarse-grid correction } \mathbf{u}_l = \mathbf{u}_l + \mathcal{P}(\mathbf{w} - \mathbf{v}). \\ &\quad \text{Do } \nu_2 \text{ post-smoothing iterations } \mathbf{u}_l \leftarrow \mathcal{S}_l^{(\nu_2)}(\mathbf{u}_l, \mathbf{g}_l). \\ &\text{End.} \end{aligned} \quad (3.16)$$

The terms pre- and post-smoothing refer to the nonlinear, block Gauss–Seidel iterations performed before and after coarse-grid correction, respectively. Parameters  $\nu_1$ ,  $\nu_2$  and  $M$  are defined by the user. In our implementation,  $\nu_1 = 2$ ,  $\nu_2 = 0$  and  $M = 2$ . The second version of **NMGM**, introduced in [24], is a slight modification of (3.16), which uses coarse-grid solutions

$\mathbf{u}_{l-1}$  calculated in advance.

Suppose that  $\mathbf{u}_k$  and  $\mathbf{g}_k = \mathcal{L}_k(\mathbf{u}_k)$ , for  $k = 0, 1, \dots, l-1$ , are known.

Procedure **NMGM**( $l, \mathbf{u}_l, \mathbf{g}_l$ ) :

If  $l = 0$ ,

$$\mathbf{u}_l = \mathcal{L}_0^{-1}(\mathbf{g}_l).$$

Else,

$$\text{do } \nu_1 \text{ pre-smoothing iterations } \mathbf{u}_l \leftarrow \mathcal{S}_l^{(\nu_1)}(\mathbf{u}_l, \mathbf{g}_l),$$

$$\mathbf{d} = \mathbf{g}_l - \tau \mathcal{R}[\mathbf{g}_l - \mathcal{L}_l(\mathbf{u}_l)], \quad (3.17)$$

$$\mathbf{w} = \mathbf{u}_{l-1}.$$

Call **NMGM**( $l-1, \mathbf{w}, \mathbf{d}$ )  $M \geq 2$  times.

$$\text{Do coarse-grid correction } \mathbf{u}_l = \mathbf{u}_l + \frac{1}{\tau} \mathcal{P}(\mathbf{w} - \mathbf{u}_{l-1}).$$

$$\text{Do } \nu_2 \text{ post-smoothing iterations } \mathbf{u}_l \leftarrow \mathcal{S}_l^{(\nu_2)}(\mathbf{u}_l, \mathbf{g}_l).$$

End.

Version (3.17) is more convenient for analysis, due to the extra parameter  $\tau$  that can be chosen in such a way that  $\mathbf{d}$ , needed for the coarse-grid correction, is sufficiently small (see section 6.2.1). Nevertheless, for our problem, numerical experiments show that, with a proper  $\tau$ , (3.16) and (3.17) have a similar performance.

We conclude this section with an explanation of the coarse-grid correction. The analysis of versions (3.16) and (3.17) is similar, so we consider the FAS algorithm (3.16). After  $\nu_1$  pre-smoothing iterations, the residual on grid  $G_l$  is given by

$$\mathbf{r}_l = \mathbf{g}_l - \mathcal{L}_l(\mathbf{u}_l), \quad (3.18)$$

and the error is

$$\delta \mathbf{u}_l = \mathcal{L}_l^{-1}(\mathbf{g}_l) - \mathcal{L}_l^{-1}(\mathbf{g}_l - \mathbf{r}_l) = L_l^{-1}(\mathcal{L}_l^{-1}(\mathbf{g}_l))\mathbf{r}_l + \mathcal{O}(\|\mathbf{r}_l\|^2), \quad (3.19)$$

where  $L_l(\mathcal{L}_l^{-1}(\mathbf{g}_l))$  is the Jacobian of  $\mathcal{L}_l$ , calculated at the solution of (3.13). The computation of  $\delta \mathbf{u}_l$  from (3.19) is too expensive. However,  $\delta \mathbf{u}_l$  is smooth (due to pre-smoothing) and thus it can be approximated by  $\delta \tilde{\mathbf{u}}_l$  on the coarser grid  $G_{l-1}$ . Algorithm (3.16) gives

$$\delta \tilde{\mathbf{u}}_l = \mathcal{P}(\mathbf{w} - \mathbf{v}) = \mathcal{P}[\mathcal{L}_{l-1}^{-1}(\mathbf{d}) - \mathcal{R}\mathbf{u}_l], \quad (3.20)$$

where

$$\mathcal{L}_{l-1}^{-1}(\mathbf{d}) = \mathcal{L}_{l-1}^{-1}(\mathcal{L}_{l-1}(\mathcal{R}\mathbf{u}_l) + \mathcal{R}\mathbf{r}_l) = \mathcal{R}\mathbf{u}_l + L_{l-1}^{-1}(\mathcal{R}\mathbf{u}_l)\mathcal{R}\mathbf{r}_l + \mathcal{O}(\|\mathbf{r}_l\|^2). \quad (3.21)$$

Hence, the coarse-grid correction is

$$\delta \tilde{\mathbf{u}}_l = \mathcal{P}L_{l-1}^{-1}(\mathcal{R}\mathbf{u}_l)\mathcal{R}\mathbf{r}_l + \mathcal{O}(\|\mathbf{r}_l\|^2), \quad (3.22)$$

an approximation of (3.19).

### 3.3. Acceleration of coarse-grid correction in the FAS algorithm

After  $\nu_1$  relaxation sweeps, procedure **NMGM**, given by (3.16), takes  $\mathbf{u}_l$  and residual  $\mathbf{r}_l = \mathbf{g}_l - \mathcal{L}_l(\mathbf{u}_l)$ , and projects them on  $G_{l-1}$ , for the purpose of coarse-grid correction. Since the nested iteration algorithm (3.12) makes  $\tilde{M}$  repeated calls of **NMGM**, we have a sequence of admittivities  $\mathbf{u}_l$ . At step  $j = 1, 2, \dots, \tilde{M}$ , let us denote by  $\tilde{\mathbf{u}}_l^j$  the admittivity obtained after  $\nu_1$  pre-smoothing iterations. We can speed up the convergence of (3.16) by using the *minimal residual smoothing* (MRS) acceleration technique [47, 48], where we project on

$G_{l-1}$  the linear combination  $\beta \tilde{\mathbf{u}}_l^j + (1 - \beta) \tilde{\mathbf{u}}_l^{j-1}$ . The acceleration parameter  $\beta$  is chosen such that the new admittivity minimizes the Euclidian norm of the residual.

Suppose that, in nested iteration (3.12), we have reached level  $\tilde{l}$ , where  $1 \leq \tilde{l} \leq K$ . At this level, for  $j = 1, \dots, \tilde{M}$ , we call procedure **NMGM**. To accelerate convergence, we modify (3.16) as

$$\begin{aligned}
& \text{Procedure } \mathbf{NMGM}(l, \mathbf{u}_l, \mathbf{g}_l): \\
& \text{If } l = 0, \\
& \quad \mathbf{u}_l = \mathcal{L}_0^{-1}(\mathbf{g}_l). \\
& \text{Else,} \\
& \quad \mathbf{u}_l \leftarrow \mathcal{S}_l^{(v_1)}(\mathbf{u}_l, \mathbf{g}_l), \\
& \quad \mathbf{r}_l = \mathbf{g}_l - \mathcal{L}_l(\mathbf{u}_l). \\
& \quad \text{If } l = \tilde{l}, \\
& \quad \quad \tilde{\mathbf{u}}_l^j = \mathbf{u}_l. \\
& \quad \quad \text{If } j > 1, \\
& \quad \quad \quad \text{given } \beta, \text{ a minimizer of } \|\mathbf{g}_l - \mathcal{L}_l(\beta \tilde{\mathbf{u}}_l^j + (1 - \beta) \tilde{\mathbf{u}}_l^{j-1})\|_2^2, \\
& \quad \quad \quad \tilde{\mathbf{u}}_l^j = \beta \tilde{\mathbf{u}}_l^j + (1 - \beta) \tilde{\mathbf{u}}_l^{j-1}, \\
& \quad \quad \quad \mathbf{u}_l = \tilde{\mathbf{u}}_l^j, \\
& \quad \quad \quad \mathbf{r}_l = \mathbf{g}_l - \mathcal{L}_l(\mathbf{u}_l), \\
& \quad \quad \text{end.} \\
& \quad \text{End.} \\
& \quad \mathbf{v} = \mathcal{R}\mathbf{u}_l, \\
& \quad \mathbf{d} = \mathcal{L}_{l-1}(\mathbf{v}) + \mathcal{R}\mathbf{r}_l, \\
& \quad \mathbf{w} = \mathbf{v}. \\
& \quad \text{Call } \mathbf{NMGM}(l - 1, \mathbf{w}, \mathbf{d}) \text{ } M \geq 2 \text{ times.} \\
& \quad \mathbf{u}_l = \mathbf{u}_l + \mathcal{P}(\mathbf{w} - \mathbf{v}), \\
& \quad \mathbf{u}_l \leftarrow \mathcal{S}_l^{(v_2)}(\mathbf{u}_l, \mathbf{g}_l). \\
& \quad \text{End.}
\end{aligned} \tag{3.23}$$

In our implementation, we solve the nonlinear, one-dimensional minimization problem for  $\beta$ , with the MATLAB function *fminbnd*.

The MRS acceleration is done only at the highest level  $\tilde{l}$ , reached in iteration (3.12), where  $\mathbf{g}_{\tilde{l}} = \mathbf{0}$  holds. On grids  $G_l$ , where  $l = 1, \dots, \tilde{l} - 1$ , we are solving  $\mathcal{L}_l(\mathbf{u}_l) = \mathbf{g}_l$ , for the purpose of correcting the solution on  $G_{\tilde{l}}$  and, the right-hand side  $\mathbf{g}_l$  on  $G_l$ , given by a vector  $\mathbf{d}$  such as in (3.23), changes at each iteration. This means that the smoothed  $\mathbf{u}_l$  from the previous iteration has nothing to do with  $\mathbf{u}_l$  of the current iteration and the MRS acceleration technique does not apply to the intermediate grids. Note however that, for coarse-grid correction, procedure **NMGM** is called  $M$  times, with the same right-hand side  $\mathbf{d}$ . Hence, we can define shorter sequences of admittivities on the intermediate grids and use the MRS technique for acceleration. In our numerical experiments, we take  $M = 2$ , so we have no intermediate-grid acceleration.

#### 4. The coarse-grid solution

As shown in [24] and section 6, an essential requirement for a successful multigrid iteration is that the approximation property  $\mathcal{L}_l^{-1}(\mathbf{g}_l) - \mathcal{P}\mathcal{L}_{l-1}^{-1}(\mathcal{R}\mathbf{g}_l) = O(h_l^p)$  hold, for some  $p > 0$ .

In particular, this means that  $\rho^{(l-1)}$ , the solution of (3.4) on  $G_{l-1}$  must be ‘close’ to  $\rho^{(l)}$ , the solution on  $G_l$ .

In section 3.1, we describe the piecewise linear, finite-element method used to calculate  $\phi_j$  and  $\psi_j$  and, implicitly, the nonlinear part of  $\mathcal{F}_l$  or  $\mathcal{L}_l$ . The accuracy of  $\nabla\phi_j$  and  $\nabla\psi_j$  is  $O(h_l)$ , provided that the excitation current  $I_j$  at  $\partial\Omega$  is smooth [27]. On the coarse grids, especially on  $G_0$ , where the grid spacing can be quite large, we expect a significant error in the calculation of both  $\nabla\phi_j \cdot \nabla\psi_j$  and the misfit  $\phi_j - V_j$  at the boundary. Due to the ill-posedness of the inverse problem, the error in the boundary misfit  $\phi_j|_{\partial\Omega} - V_j$  is highly amplified in the image of the admittivity in the interior of  $\Omega$ . To obtain a reasonable  $\rho^{(l)}$  on a coarse grid, we need a large regularization parameter which leads to unsatisfactory, blurry images.

One possible way of ameliorating this problem is to use a higher-order numerical scheme for the solution of (2.9) and (2.14), on the coarse grids. In the finite-element setting, this means interpolating  $\phi_j$ ,  $\psi_j$  and  $\rho^{(l)}$  by higher-degree polynomials. For example, suppose that, on the triangulation  $\mathcal{T}_0$ , we take a piecewise quadratic interpolation of  $\phi_j$  and the admittivity. Then, the vector of unknowns in (3.7) contains values of  $\phi_j$  at  $(x_i, y_j) \in \overline{G}_0$  as well as at additional points, such as  $(x_i + \frac{h_0}{2}, y_j)$ ,  $(x_i, y_j + \frac{h_0}{2})$ ,  $(x_i + \frac{h_0}{2}, y_j + \frac{h_0}{2})$ . Similarly, a piecewise quadratic interpolation of the admittivity causes matrix  $A^{(0)}$  in (3.7) to depend not only on  $\rho^{(0)}$ , the restriction of  $\rho$  at  $(x_i, y_j) \in \overline{G}_0$  but also on  $\rho(x_i + \frac{h_0}{2}, y_j)$ ,  $\rho(x_i, y_j + \frac{h_0}{2})$  and  $\rho(x_i + \frac{h_0}{2}, y_j + \frac{h_0}{2})$ . Hence, the discretization (3.4) at level  $l = 0$  becomes dependent on the discretization on the next grid,  $G_1$ , and the computational cost on  $G_0$  is too high. A high-order finite-difference scheme could be used to solve (2.9) and (2.14), as well, but the accuracy of the result would be highly dependent on the smoothness of  $I_j(x)$ . Finally, it is most convenient to have the same numerical method for the solution of (2.9) and (2.14) on all grid levels.

In this section, we introduce an idea that allows us to get a good approximation of  $\rho$  on the coarse grids, without changing the numerical scheme for the solution of (2.9) and (2.14) on coarse grids and, especially, without increasing  $\alpha_l$  and thus compromising resolution.

#### 4.1. A coarse-grid least-squares problem

We assume that we know the NtD map at some or all boundary points of the finest grid  $G_K$ , and we denote by  $\mathbf{V}_j$  the vector of measured potentials  $V_j(x)$ , for  $x \in \partial G_K$ . Then, we expect that

$$\mathbf{V}_j \approx \mathbf{\Lambda}_K(\rho^{(K)})I_j, \quad (4.1)$$

where  $\mathbf{\Lambda}_K$  is the discrete NtD map for the fine grid and  $\rho^{(K)}$  is the restriction of the true admittivity on grid  $G_K$ . The ideal coarse-grid image is the restriction of  $\rho$  on  $G_0$ . Therefore, on grid  $G_0$ , we formulate the least-squares problem

$$\min_{\rho^{(0)}} \sum_{j=1}^{N_{\text{exp}}} \|\mathcal{R}_{0 \leftarrow K} \mathbf{\Lambda}_K(\mathcal{P}_{K \leftarrow 0} \rho^{(0)})I_j - \mathcal{R}_{0 \leftarrow K} \mathbf{V}_j\|_2^2 + \alpha_0 \|\nabla_{h_0} \rho^{(0)}\|_{h_0,0}^2, \quad (4.2)$$

where  $\|\nabla_{h_0} \rho^{(0)}\|_{h_0,0}$  is the discrete version of the  $L_2$  norm of  $\nabla\rho$ . By solving (4.2), we look for a solution  $\rho^{(0)}$  that is ‘close’ to the restriction of the true admittivity  $\rho$  on  $G_0$ .

The restriction operator in (4.2) is

$$\mathcal{R}_{0 \leftarrow K} = \mathcal{R}_{0 \leftarrow 1} \dots \mathcal{R}_{K-1 \leftarrow K}, \quad (4.3)$$

where  $\mathcal{R}_{l-1 \leftarrow l}$  takes functions defined at  $\partial G_l$  into functions defined at  $\partial G_{l-1}$ . We consider the weighted restriction

$$d_{l-1}(t) = \mathcal{R}_{l-1 \leftarrow l} d_l = \frac{1}{4}[d_l(t - h_l) + 2d_l(t) + d_l(t + h_l)],$$

for  $d_l$  given at  $\partial G_l$  and  $t \in \partial G_{l-1}$ . Similarly,

$$\mathcal{P}_{K \leftarrow 0} = \mathcal{P}_{K \leftarrow K-1} \dots \mathcal{P}_{1 \leftarrow 0}, \quad (4.4)$$

where  $\mathcal{P}_{l \leftarrow l-1}$  is the nine-point prolongation defined in section 3.1.

**Proposition 1.** *The following factorization holds:*

$$\mathcal{R}_{0 \leftarrow K} \Lambda_K (\mathcal{P}_{K \leftarrow 0} \rho^{(0)}) I_j = \Lambda_0 (\rho^{(0)}) \mathbf{I}_j^{(0)} (\rho^{(0)}), \quad (4.5)$$

where matrix  $\Lambda_0$  is the coarse-grid NtD map and  $\mathbf{I}_j^{(0)}$  is a vector of currents defined at  $\partial G_0$ . The definition of  $\Lambda_0$  and  $\mathbf{I}_j^{(0)}$  depends on the numerical solution of (2.9), on  $G_0$ . We choose the piecewise linear, finite-element approach described in section 3.1, where the boundary current is  $\mathcal{I}_j^{(0)} \in L_2(\partial\Omega)$ , the linear spline interpolation of the nodal values in vector  $\mathbf{I}_j^{(0)}$ .

**Proof.** Consider triangulation  $\mathcal{T}_0$  of  $\Omega$ , with vertices given by the grid points in  $\overline{G}_0$ . Let  $r^{(0)}(\mathbf{x})$  be the piecewise linear interpolation of  $\rho^{(0)}$ , given on  $\overline{G}_0$ . The finite-element solution  $\phi_j^{(0)}(\mathbf{x})$  of (2.9), with admittivity  $r^{(0)}(\mathbf{x})$  and excitation  $\mathcal{I}_j^{(0)}$ , satisfies

$$\int_{\Omega} r^{(0)}(\mathbf{x}) \nabla \phi_j^{(0)}(\mathbf{x}) \cdot \nabla \vartheta(\mathbf{x}) \, d\mathbf{x} = \int_{\partial\Omega} \vartheta(t) \mathcal{I}_j^{(0)}(t) \, dt, \quad (4.6)$$

for all piecewise linear functions  $\vartheta(t)$  defined on  $\mathcal{T}_0$ . The discretization of (4.6) leads to a linear system of equations, similar to (3.7), which we write in block form as

$$\begin{pmatrix} B^{(0)}(\rho^{(0)}) & C^{(0)}(\rho^{(0)}) \\ D^{(0)}(\rho^{(0)}) & E^{(0)}(\rho^{(0)}) \end{pmatrix} \begin{pmatrix} \phi_{j(\text{interior})}^{(0)} \\ \phi_{j(\text{boundary})}^{(0)} \end{pmatrix} = \begin{pmatrix} \mathbf{0} \\ \mathcal{Q} \mathbf{I}_j^{(0)} \end{pmatrix}, \quad (4.7)$$

where  $\phi_{j(\text{interior})}^{(0)} \in \mathbb{C}^{(n_0-1)^2}$  contains the values of  $\phi_j^{(0)}$  at the interior nodes and  $\phi_{j(\text{boundary})}^{(0)} \in \mathbb{C}^{4n_0}$  is the vector of boundary potentials. Matrices  $B^{(0)}$ ,  $C^{(0)}$ ,  $D^{(0)}$  and  $E^{(0)}$  depend linearly on  $\rho^{(0)}$ , whereas  $\mathcal{Q} \in \mathbb{R}^{4n_0 \times 4n_0}$  is a constant, nonsingular matrix.

Now, consider the Dirichlet problem

$$\begin{aligned} \int_{\Omega} r^{(0)}(\mathbf{x}) \nabla \varphi_j^{(0)}(\mathbf{x}) \cdot \nabla \vartheta(\mathbf{x}) \, d\mathbf{x} &= 0, \\ \varphi_j^{(0)}|_{\partial\Omega} &= \text{linear spline interpolation of } \mathcal{R}_{0 \leftarrow K} \Lambda_K (\mathcal{P}_{K \leftarrow 0} \rho^{(0)}) I_j, \end{aligned} \quad (4.8)$$

for all piecewise linear functions  $\vartheta(t)$  defined on  $\mathcal{T}_0$ , that vanish at  $\partial\Omega$ . We wish to calculate  $\mathbf{I}_j^{(0)}$  such that

$$\phi_{j(\text{boundary})}^{(0)} = \mathcal{R}_{0 \leftarrow K} \Lambda_K (\mathcal{P}_{K \leftarrow 0} \rho^{(0)}) I_j = \varphi_{j(\text{boundary})}^{(0)}. \quad (4.9)$$

Since  $\phi_j^{(0)}$  and  $\varphi_j^{(0)}$  solve the same equation, (4.9) implies  $\phi_{j(\text{interior})}^{(0)} = \varphi_{j(\text{interior})}^{(0)}$ , the unique solution of (4.8). Finally,  $\mathbf{I}_j^{(0)}$  is uniquely defined by

$$\mathbf{I}_j^{(0)}(\rho^{(0)}) = \mathcal{Q}^{-1} (D^{(0)}(\rho^{(0)}) \ E^{(0)}(\rho^{(0)})) \begin{pmatrix} \varphi_{j(\text{interior})}^{(0)} \\ \varphi_{j(\text{boundary})}^{(0)} \end{pmatrix} \quad (4.10)$$

and proposition 1 is proved.  $\square$

In light of proposition 1, we rewrite the coarse-grid minimization problem (4.2) as

$$\min_{\rho^{(0)}} \sum_{j=1}^{N_{\text{exp}}} \|\Lambda_0(\rho^{(0)}) \mathbf{I}_j^{(0)}(\rho^{(0)}) - \mathcal{R}_{0 \leftarrow K} \mathbf{V}_j\|_2^2 + \|\nabla_{h_0} \rho^{(0)}\|_{h_0,0}^2. \quad (4.11)$$

It appears that a numerical solution of (4.11) is very expensive because the coarse-grid current  $\mathbf{I}_j^{(0)}(\rho^{(0)})$  depends on  $\rho^{(0)}$  and, to calculate it, we must solve equation (2.9), on the fine grid

$G_K$ , for admittivity  $\mathcal{P}_{K \leftarrow 0} \rho^{(0)}$ . However, proposition 2 shows that the dependence of  $I_j^{(0)}$  on  $\rho^{(0)}$  is much weaker than that of  $\Lambda_0$ . Hence, we can solve (4.11) with only a few updates of  $I_j^{(0)}$ .

**Proposition 2.** Consider a small perturbation  $\delta\rho^{(0)}$  of  $\rho^{(0)}$ , such that  $\delta\rho^{(0)}|_{\partial G_0} = 0$ . The coarse-grid boundary values of the potential are perturbed by

$$\delta[\Lambda_0(\rho^{(0)})I_j^{(0)}(\rho^{(0)})] = \delta\Lambda_0(\rho^{(0)})I_j^{(0)}(\rho^{(0)}) + \Lambda_0(\rho^{(0)})\delta I_j^{(0)}(\rho^{(0)}),$$

where

$$\delta\Lambda_0(\rho^{(0)})I_j^{(0)}(\rho^{(0)}) \gg \Lambda_0(\rho^{(0)})\delta I_j^{(0)}(\rho^{(0)}). \quad (4.12)$$

**Proof.** As we did in the proof of proposition 1, we denote by  $r^{(0)}(\mathbf{x})$  and  $\delta r^{(0)}(\mathbf{x})$  the piecewise linear interpolation of  $\rho^{(0)}$  and  $\delta\rho^{(0)}$ , respectively. We have

$$\delta\Lambda_0(\rho^{(0)})I_j^{(0)}(\rho^{(0)}) = \delta\phi_j^{(0)}|_{\partial G_0} + \mathcal{O}(\|\delta\rho^{(0)}\|^2), \quad (4.13)$$

where  $\delta\phi_j^{(0)}$  is the finite-element solution of

$$\begin{aligned} \nabla \cdot [r^{(0)}(\mathbf{x})\nabla\delta\phi_j^{(0)}(\mathbf{x})] &= -\nabla \cdot [\delta r^{(0)}(\mathbf{x})\nabla\phi_j^{(0)}(\mathbf{x})] && \text{in } \Omega, \\ \nabla\delta\phi_j^{(0)}(\mathbf{x}) \cdot \mathbf{n}(\mathbf{x}) &= 0 && \text{on } \partial\Omega, \\ \int_{\partial\Omega} \delta\phi_j^{(0)}(s) \, ds &= 0, \end{aligned} \quad (4.14)$$

and  $\phi_j^{(0)}$  solves (4.6). Moreover,

$$\Lambda_0(\rho^{(0)})\delta I_j^{(0)}(\rho^{(0)}) = \delta\tilde{\phi}_j^{(0)}|_{\partial G_0} + \mathcal{O}(\|\delta\rho^{(0)}\|^2), \quad (4.15)$$

where  $\delta\tilde{\phi}_j^{(0)}$  is the finite-element solution of

$$\begin{aligned} \nabla \cdot [r^{(0)}(\mathbf{x})\nabla\delta\tilde{\phi}_j^{(0)}(\mathbf{x})] &= 0 && \text{in } \Omega, \\ r^{(0)}(\mathbf{x})\nabla\delta\tilde{\phi}_j^{(0)}(\mathbf{x}) \cdot \mathbf{n}(\mathbf{x}) &= \delta\mathcal{I}_j^{(0)}(\mathbf{x}) && \text{on } \partial\Omega, \\ \int_{\partial\Omega} \delta\tilde{\phi}_j^{(0)}(s) \, ds &= 0. \end{aligned} \quad (4.16)$$

Current density  $\delta\mathcal{I}_j^{(0)}$  is the linear spline interpolation of the nodal values in vector  $\delta I_j^{(0)}$ , given by

$$\begin{aligned} \delta I_j^{(0)}(\rho^{(0)}) &= \mathcal{Q}^{-1} \left[ \begin{array}{c} (\delta D^{(0)}(\rho^{(0)}) \quad \delta E^{(0)}(\rho^{(0)})) \begin{pmatrix} \varphi_j^{(0)}(\text{interior}) \\ \varphi_j^{(0)}(\text{boundary}) \end{pmatrix} \\ + (D^{(0)}(\rho^{(0)}) \quad E^{(0)}(\rho^{(0)})) \begin{pmatrix} \delta\varphi_j^{(0)}(\text{interior}) \\ \delta\varphi_j^{(0)}(\text{boundary}) \end{pmatrix} \end{array} \right], \end{aligned} \quad (4.17)$$

where  $\varphi_j^{(0)}$  and  $\delta\varphi_j^{(0)}$  are the finite-element solutions of (4.8) and

$$\begin{aligned} \nabla \cdot [r^{(0)}(\mathbf{x})\nabla\delta\varphi_j^{(0)}(\mathbf{x})] &= -\nabla \cdot [\delta r^{(0)}(\mathbf{x})\nabla\varphi_j^{(0)}(\mathbf{x})] && \text{in } \Omega, \\ \delta\varphi_j^{(0)}|_{\partial\Omega} &= \text{linear spline interpolation of } \mathcal{R}_{0 \leftarrow K} \delta\Lambda_K(\mathcal{P}_{K \leftarrow 0} \rho^{(0)})I_j, \end{aligned} \quad (4.18)$$

respectively.

On the finest grid  $G_K$ , we denote by  $r^{(K)}(\mathbf{x})$  and  $\delta r^{(K)}(\mathbf{x})$  the piecewise linear interpolation of  $\mathcal{P}_{K \leftarrow 0} \rho^{(0)}$  and  $\mathcal{P}_{K \leftarrow 0} \delta\rho^{(0)}$ , on triangulation  $\mathcal{T}_K$ . Suppose that  $\phi_j^{(K)}$  is the fine-grid, finite-element solution of (2.9), with admittivity  $r^{(K)}(\mathbf{x})$  and known excitation current  $I_j(\mathbf{x})$ . We have

$$\delta\Lambda_K(\mathcal{P}_{K \leftarrow 0} \rho^{(0)})I_j = \delta\phi_j^{(K)}|_{\partial G_K} + \mathcal{O}(\|\delta\rho^{(0)}\|^2), \quad (4.19)$$

where  $\delta\phi_j^{(K)}$  is the finite-element solution of

$$\begin{aligned} \nabla \cdot [r^{(K)}(\mathbf{x})\delta\nabla\phi_j^{(K)}(\mathbf{x})] &= -\nabla \cdot [\delta r^{(K)}(\mathbf{x})\nabla\phi_j^{(K)}(\mathbf{x})] & \text{in } \Omega, \\ \nabla\delta\phi_j^{(K)} \cdot \mathbf{n}(\mathbf{x}) &= 0 & \text{on } \partial\Omega, \end{aligned} \quad (4.20)$$

on grid  $G_K$ . The discretization of (4.20) leads to a linear system of equations which we write in block form as

$$\begin{aligned} \begin{pmatrix} \delta B^{(K)}(\mathcal{P}_{K \leftarrow 0}\rho^{(0)}) & \delta C^{(K)}(\mathcal{P}_{K \leftarrow 0}\rho^{(0)}) \\ \delta D^{(K)}(\mathcal{P}_{K \leftarrow 0}\rho^{(0)}) & \delta E^{(K)}(\mathcal{P}_{K \leftarrow 0}\rho^{(0)}) \end{pmatrix} \begin{pmatrix} \phi_j^{(K)}(\text{interior}) \\ \phi_j^{(K)}(\text{boundary}) \end{pmatrix} \\ + \begin{pmatrix} B^{(K)}(\mathcal{P}_{K \leftarrow 0}\rho^{(0)}) & C^{(K)}(\mathcal{P}_{K \leftarrow 0}\rho^{(0)}) \\ D^{(K)}(\mathcal{P}_{K \leftarrow 0}\rho^{(0)}) & E^{(K)}(\mathcal{P}_{K \leftarrow 0}\rho^{(0)}) \end{pmatrix} \begin{pmatrix} \delta\phi_j^{(K)}(\text{interior}) \\ \delta\phi_j^{(K)}(\text{boundary}) \end{pmatrix} &= \mathbf{0}. \end{aligned} \quad (4.21)$$

Here, matrices  $B^{(K)}$ ,  $C^{(K)}$ ,  $D^{(K)}$  and  $E^{(K)}$  depend linearly on the admittivity, and they are similar to  $B^{(0)}$ ,  $C^{(0)}$ ,  $D^{(0)}$  and  $E^{(0)}$  in (4.7).

At last, we note that, by construction, at  $\partial G_0$ ,  $\phi_j^{(0)}$  is the restriction of  $\phi_j^{(K)}$ . Moreover, the fine-grid potential  $\phi_j^{(K)}$  corresponds to an admittivity  $\mathcal{P}_{K \leftarrow 0}\rho^{(0)}$  that is a linear interpolation of  $\rho^{(0)}$ . On both grids  $G_0$  and  $G_K$ , we are discretizing the same elliptic operator and the discretization is consistent. This implies that the perturbation current in (4.17) is approximately

$$\begin{aligned} \delta\mathbf{I}_j^{(0)}(\rho^{(0)}) &\approx \mathcal{Q}^{-1}\mathcal{R}_{0 \leftarrow K} \left[ \begin{aligned} &(\delta D^{(K)}(\mathcal{P}_{K \leftarrow 0}\rho^{(0)}) \quad \delta E^{(K)}(\mathcal{P}_{K \leftarrow 0}\rho^{(0)})) \begin{pmatrix} \phi_j^{(K)}(\text{interior}) \\ \phi_j^{(K)}(\text{boundary}) \end{pmatrix} \\ &+ (D^{(K)}(\mathcal{P}_{K \leftarrow 0}\rho^{(0)}) \quad E^{(K)}(\mathcal{P}_{K \leftarrow 0}\rho^{(0)})) \begin{pmatrix} \delta\phi_j^{(K)}(\text{interior}) \\ \delta\phi_j^{(K)}(\text{boundary}) \end{pmatrix} \end{aligned} \right] = \mathbf{0} \end{aligned}$$

and so  $\Lambda_0(\rho^{(0)})\delta\mathbf{I}_j^{(0)}(\rho^{(0)}) \approx \mathcal{O}(\|\delta\rho^{(0)}\|^2)$  is much smaller than  $\delta\Lambda_0(\rho^{(0)})\mathbf{I}_j^{(0)}(\rho^{(0)}) = \mathcal{O}(\|\delta\rho^{(0)}\|)$ .

To illustrate the statement of proposition 2, we show next a numerical comparison of  $\delta\Lambda_0\mathbf{I}_j^{(0)}$  and  $\Lambda_0\delta\mathbf{I}_j^{(0)}$ . Consider an admittivity  $\rho^{(0)}$  with real and imaginary parts shown in figures 1 and 2. We perturb  $\rho^{(0)}$  by  $\delta\rho^{(0)}$ , where

$$\delta\rho^{(0)}(x_i, y_j) = \begin{cases} 0.1 & \text{if } (x_i, y_j) = (4h_0, 3h_0) \\ 0.1i & \text{if } (x_i, y_j) = (3h_0, 5h_0) \\ 0 & \text{otherwise.} \end{cases}$$

The real parts of  $\delta\Lambda_0\mathbf{I}_j^{(0)}$  and  $\Lambda_0\delta\mathbf{I}_j^{(0)}$  are shown in figures 3 and 4, where we take two different current excitations  $I_j$  on the fine grid. The comparison between the imaginary parts is similar to that in figures 3 and 4. As predicted by proposition 2, perturbation  $\delta\Lambda_0\mathbf{I}_j^{(0)}$  is indeed much stronger than  $\Lambda_0\delta\mathbf{I}_j^{(0)}$ .  $\square$

#### 4.2. Numerical algorithm for coarse-grid solution

Nested iteration (3.12) begins with the coarse-grid admittivity  $u_0 \approx \mathcal{L}_0^{-1}(\mathbf{0})$ , which we calculate as follows: We start with the initial guess  $\rho^{(0)}$  given by the restriction on  $G_0$  of the harmonic extension inside  $\Omega$ , of the known admittivity at the boundary. For this  $\rho^{(0)}$ , we calculate the coarse-grid currents  $\mathbf{I}_j^{(0)}$ , for  $j = 1, \dots, N_{\text{exp}}$ , as explained in proposition 1. Given the sensitivity analysis of proposition 2, we update  $\rho^{(0)}$  a couple of times, without

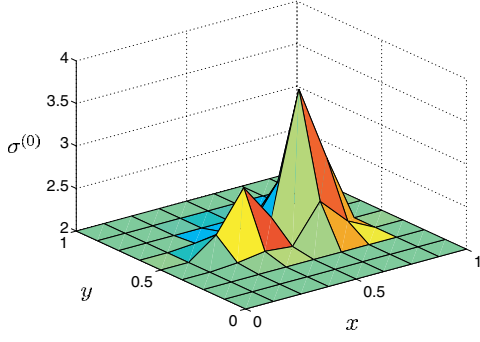


Figure 1. Real part of admittivity  $\rho^{(0)}$ .

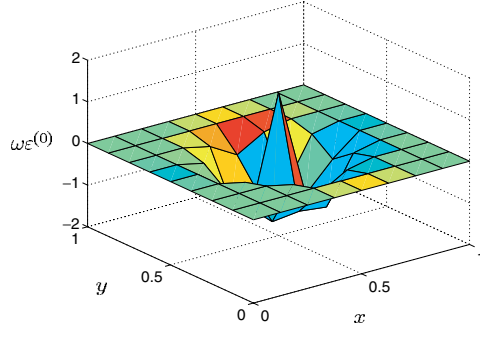


Figure 2. Imaginary part of  $\rho^{(0)}$ .

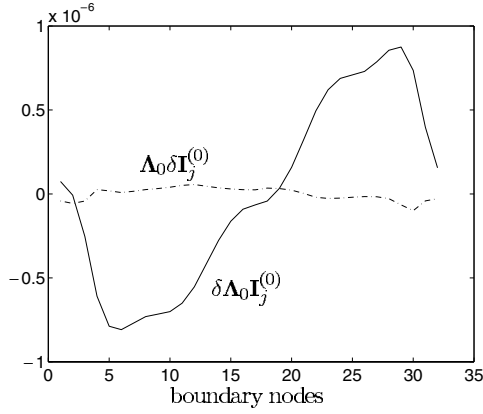


Figure 3. Real part of the perturbation of the boundary potential due to  $\delta\rho^{(0)}$ . Experiment 1.

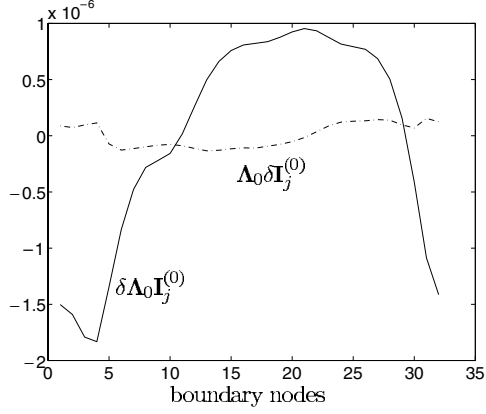


Figure 4. Real part of the perturbation of the boundary potential due to  $\delta\rho^{(0)}$ . Experiment 2.

changing  $I_j^{(0)}$ . Then, we recalculate the coarse-grid currents, make a couple of updates on  $\rho^{(0)}$  and so on. The algorithm that we implemented is

Get  $\rho^{(0)}$  and, implicitly,  $\mathbf{u}_0$ , the initial guess.

Set regularization parameter  $\alpha_0$  to a sufficiently large value.

For  $k = 1, 2, \dots$

Calculate coarse-grid currents  $I_j^{(0)}(\rho^{(0)})$ ,  $j = 1, \dots, N_{\text{exp}}$ ,  
as explained in proposition 1.

Solve  $\mathcal{L}_0(\alpha_0, \mathbf{u}_0) = 0$ . In the evaluation of  $\mathcal{L}_0(\alpha_0, \mathbf{u}_0)$ ,  
use  $\phi_j^{(0)}$  given by (4.7). (4.22)

To calculate the adjoint potential  $\psi_j^{(0)}$ ,

use the adjoint current  $\phi_j^{(0)}|_{\partial G_0} - \mathcal{R}_{0 \leftarrow K} \mathbf{V}_j$ .

Decrease  $\alpha_0$ .

End.

For a given  $\alpha_0$  and fixed coarse-grid currents, we solve  $\mathcal{L}_0(\alpha_0, \mathbf{u}_0) = 0$  with a Newton-type method, implemented in the public domain software *hybrj* [22]. Note that we start the coarse-

grid iteration with a large regularization parameter  $\alpha_0$  and we reduce it as we go along. The motivation for this iterative regularization approach is that, in the beginning, we expect to have a poor guess of the solution. This means that, in factorization (4.5), we can have coarse-grid currents that are very different from  $I_j^{(0)}(\rho^{*(0)})$ , where  $\rho^{*(0)}$  is the restriction of the true  $\rho$ , on  $G_0$ . Hence, as discussed at the beginning of section 4, we need a large  $\alpha_0$  to stabilize the coarse-grid inversion. As we iterate, we expect  $\rho^{(0)}$  to get closer to  $\rho^{*(0)}$ , so we decrease the regularization parameter. In our numerical experiments,  $\alpha_0$  is reduced by a factor of 1.5 at each iteration. We terminate iteration (4.22) over  $k$  by asking that the relative change in  $\mathbf{u}_0$  at two consecutive iterations is less than or equal to  $10^{-3}$ .

Numerical algorithm (4.22) is used only once, at the beginning of nested iteration (3.12). Then, we interpolate  $\mathbf{u}_0$  on  $G_l$ , for  $l = 1, \dots, K - 1$ , and calculate the currents on  $G_l$ , by proceeding as in proposition 1. These currents are needed in the calculation of  $\phi_j^{(l)}$  and  $\psi_j^{(l)}$ , as well as the evaluation of  $\mathcal{L}_l(\mathbf{u}_l)$  on  $G_l$ . As the admittivity on the intermediate grid levels is updated, it may be useful to recalculate the coarse-grid currents from time to time. However, in all the numerical tests that we tried, we found that such additional current corrections were not really necessary. That is, as stated in proposition 2, the coarse-grid currents change very slowly with the admittivity and this allows us to get good coarse-grid images with a small number of fine-grid function evaluations. In fact, in all our experiments, after getting  $\mathbf{u}_0$ , we fix the currents on  $G_l$ , where  $l = 0, 1, \dots, K - 1$ , for the entire duration of the multigrid iteration.

## 5. Numerical results

In all numerical calculations, we consider a unit square domain  $\Omega$  and a sequence of three, uniform grids, with spacing  $h_l = \frac{1}{2^{l+3}}$ , where  $l = 0, 1, 2$ . For inversion, we take  $N_{\text{exp}} = 27$  excitation currents  $I_j$ , that satisfy  $\int_{\partial\Omega} I_j(s) ds = 0$ , and  $I_j(\mathbf{x}) = 0$  for  $\mathbf{x}$  in the vicinity of the corners of  $\Omega$ . Given any  $I_j$ , consider the restriction  $\tilde{\mathcal{R}}_{0 \leftarrow K} I_j$ , which is simple injection from  $\partial\Omega$  to  $\partial G_0$ . We have chosen currents  $I_j$  such that the coarse-grid currents in sequence  $\{\tilde{\mathcal{R}}_{0 \leftarrow K} I_j\}_{j=1}^{27}$  are linearly independent. That is, we have a complete set of currents on  $\partial G_0 \setminus \{(0, 0), (0, 1), (1, 0), (1, 1)\}$ . Note that the sole purpose of mentioning  $\tilde{\mathcal{R}}_{0 \leftarrow K} I_j$  is to explain the geometrical configuration of the current excitations  $I_j$ . Restrictions  $\tilde{\mathcal{R}}_{0 \leftarrow K} I_j$  are not used in the calculations. Instead, the coarse-grid currents are obtained from  $I_j$ , as explained in proposition 1.

For any excitation  $I_j$ , the resulting voltage  $V_j$  is given at all boundary nodes in  $\partial G_2$ , except the corners of  $\Omega$ . We have synthetic data, where we calculate potential  $\phi_j$  by solving forward problem (2.9), for all  $I_j$ ,  $j = 1, \dots, 27$ , on the fine grid  $G_2$ . The forward problem solver is the piecewise linear, finite-element numerical scheme described in section 3.1. Data  $V_j$  are the restriction of  $\phi_j$  on  $\partial G_2$ , to which we usually add random, Gaussian, multiplicative noise.

In the multigrid procedure **NMGM** defined by (3.16) or (3.17), we take  $\nu_1 = 2$  pre-smoothing iterations and no post-smoothing ( $\nu_2 = 0$ ). For coarse-grid correction, we call **NMGM**, recursively,  $M = 2$  times. In all experiments that we tried, choice  $\tau = 0.1$  in version (3.17) proved successful. In fact, we found that versions (3.16) and (3.17) of **NMGM** behaved quite similarly. However, we prefer the FAS version (3.16), because it can be accelerated, as shown in (3.23). All numerical results of this section are obtained with procedure **NMGM**, given by (3.23).

We illustrate the performance of our algorithm by reconstructing the true admittivity function  $\rho(\mathbf{x})$  with real and imaginary parts shown in figures 5 and 6.

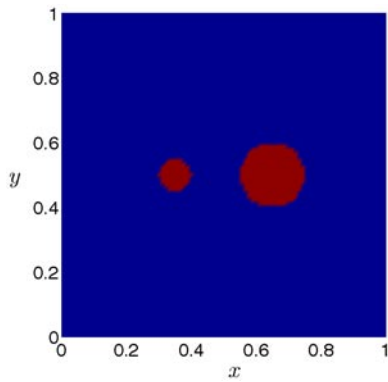


Figure 5. Real part of true  $\rho(x)$ .

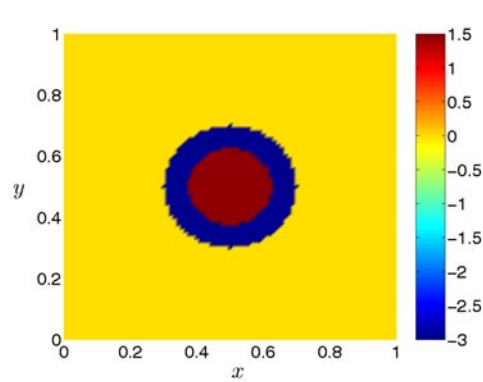


Figure 6. Imaginary part of true  $\rho(x)$ .

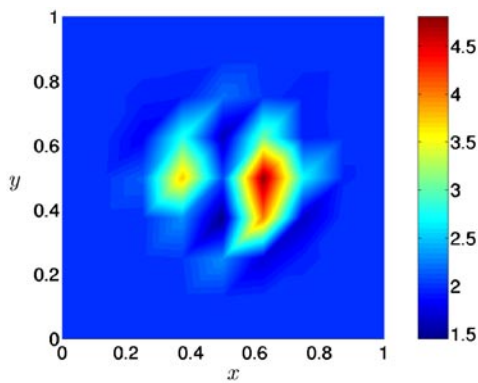


Figure 7. Real part of coarse-grid image  $\rho^{(0)}$  calculated with algorithm (4.22). Noiseless data.

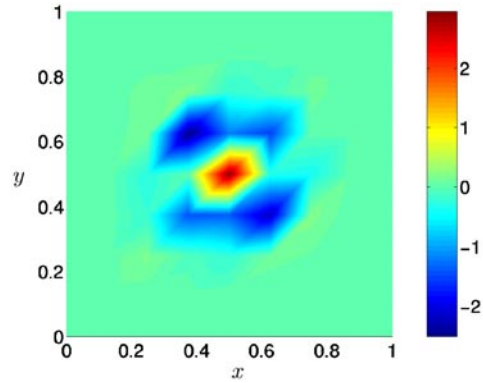
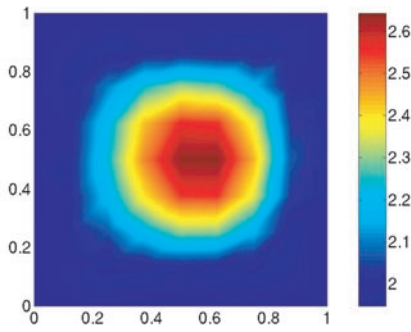


Figure 8. Imaginary part of coarse-grid image  $\rho^{(0)}$  calculated with algorithm (4.22). Noiseless data.

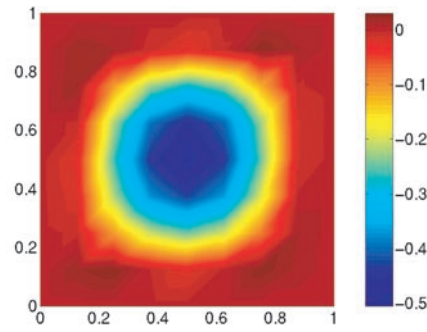
### 5.1. Noiseless data

First, we consider noiseless data. The coarse-grid image  $\rho^{(0)}$  shown in figures 7 and 8 is obtained with algorithm (4.22). At the boundary, the true admittivity is  $\rho(x) = 2$  and its harmonic extension inside  $\Omega$  is a constant, equal to 2, as well. Hence, we start algorithm (4.22) with initial guess  $\rho^{(0)}(x) = 2$ , for all  $x \in \bar{G}_0$ . The starting value of  $\alpha_0$  in (4.22) is  $10^{-6}$  and, at each iteration,  $\alpha_0$  is reduced by a factor of 1.5. For  $\alpha_0 \in [10^{-10}, 10^{-11}]$ , the image  $\rho^{(0)}$  remained practically unchanged, so we stopped the iteration when  $\alpha_0$  became smaller than  $10^{-11}$ . Figures 7 and 8 demonstrate a very good reconstruction of the coarse grid restriction of the true admittivity.

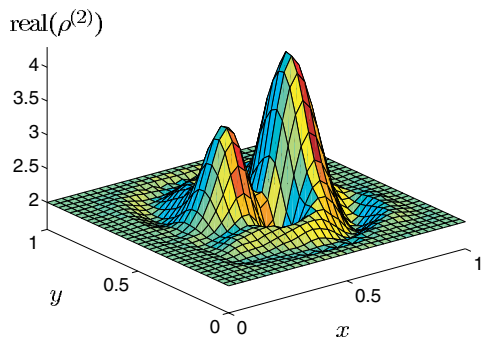
For comparison, in figures 9 and 10, we show the coarse-grid image calculated directly with the given data currents  $\{I_j\}_{j=1}^{27}$ , and a regularization parameter  $\alpha_0 = 10^{-7}$ . That is, to evaluate  $\mathcal{L}_0(u_0)$ , we solve equation (2.9) on  $G_0$ , where, instead of calculating the coarse-grid currents as in proposition 1, we simply take the given data  $\{I_j\}_{j=1}^{27}$ , known at  $\partial G_2$ . The resulting image is clearly far inferior to that given by algorithm (4.22). The two conductive peaks of the real part of the admittivity cannot be distinguished. Instead, figure 9 shows a blurry, large conductive region, where the two peaks of  $\text{real}(\rho)$  are merged together. Furthermore, figure 10 does not show the large imaginary part of  $\rho$  in the centre of  $\Omega$ . It may appear that the blurry coarse-grid



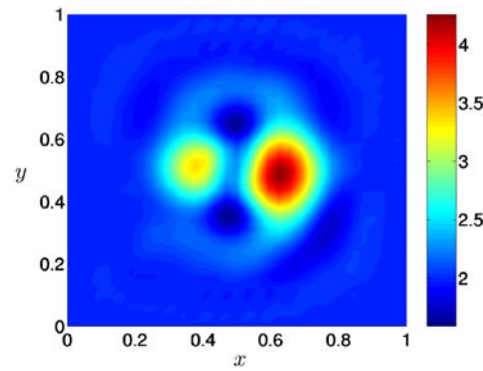
**Figure 9.** Real part of coarse-grid image  $\rho^{(0)}$ . No use of ideas in section 4.



**Figure 10.** Imaginary part of coarse grid image  $\rho^{(0)}$ . No use of ideas in section 4.



**Figure 11.** Real part of fine-grid image  $\rho^{(2)}$ . Noiseless data.



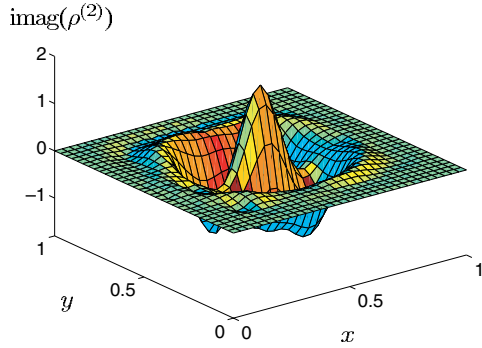
**Figure 12.** Real part of fine-grid image  $\rho^{(2)}$ . Noiseless data.

image in figures 9 and 10 might be improved by reducing  $\alpha_0$ . However, our experiments show quite the opposite. For example,  $\alpha_0 = 10^{-8}$  gives a  $\rho^{(0)}$  that is highly oscillatory, and its real part even becomes negative at some grid points in  $G_0$ . Such difficulties have been observed in all our numerical experiments and they are, in fact, what we expect. As explained in section 4, the inaccurate coarse-grid solution of equation (2.9) and the ill-posedness of the inverse problem force us to take a large regularization parameter in order to get a reasonable (although blurry) coarse-grid image. In contrast, the ideas of section 4, implemented in algorithm (4.22), lead to a much improved image on  $G_0$ , as shown in figures 7 and 8.

The regularization parameter on the intermediate grid  $G_1$  is  $\alpha_1 = 10^{-10}$ . Finally, the image on  $G_2$  is shown in figures 11–14. The regularization parameter on  $G_2$  is  $\alpha_2 = 5 \times 10^{-10}$ . Note that we have done reconstructions with various regularization parameters and found that  $\alpha_2 < 10^{-10}$  give oscillatory images of  $\rho^{(2)}$ , whereas  $\alpha_2 > 10^{-8}$  give a  $\rho^{(2)}$  that is too smooth.

The progress of nested iteration algorithm (3.12), with **NMGM** given by (3.23) is as follows:

- Initial guess  $\rho(x) = 2$  in  $\Omega$ .
- Initial residual on fine grid:  $\|\mathcal{L}_2(u_2)\|_2 = 5.073\,4578e - 2$ .



**Figure 13.** Imaginary part of fine-grid image  $\rho^{(2)}$ . Noiseless data.

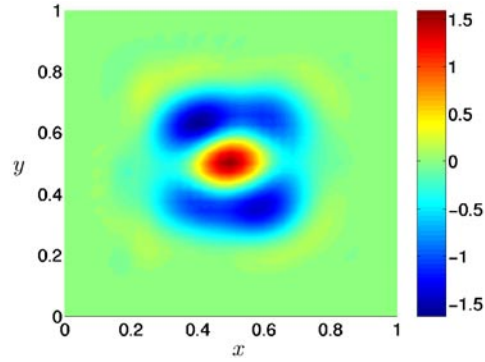


**Figure 14.** Imaginary part of fine-grid image  $\rho^{(2)}$ . Noiseless data.

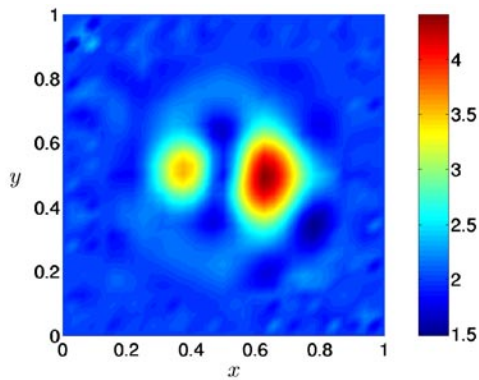
Solve coarse-grid problem and begin nested iteration (3.12):

Level $l = 1$	$\ \mathcal{L}_1(u_1)\ _2$	$\ \mathcal{L}_1(u_1)\ _\infty$
Starting residual:	1.213 5012e-4	1.422 9616e-5
After two smoothing iterations:	9.359 0648e-6	3.391 9214e-6
After coarse-grid correction:	5.288 1029e-6	1.279 5960e-6
After two smoothing iterations:	3.439 1389e-6	8.371 9534e-7
After coarse-grid correction:	1.986 1185e-6	4.166 3785e-7
Level $l = 2$	$\ \mathcal{L}_2(u_2)\ _2$	$\ \mathcal{L}_2(u_2)\ _\infty$
Starting residual:	1.821 7390e-4	1.176 5655e-5
After two smoothing iterations:	5.918 4359e-5	1.039 8852e-5
After coarse-grid correction:	3.239 9215e-5	3.967 1256e-6
After two smoothing iterations:	1.448 7300e-5	3.156 2202e-6
After coarse-grid correction:	1.234 0064e-5	2.854 5680e-6
After two smoothing iterations:	1.042 7207e-5	1.214 2867e-6
After coarse-grid correction:	9.820 3521e-6	8.713 5490e-7

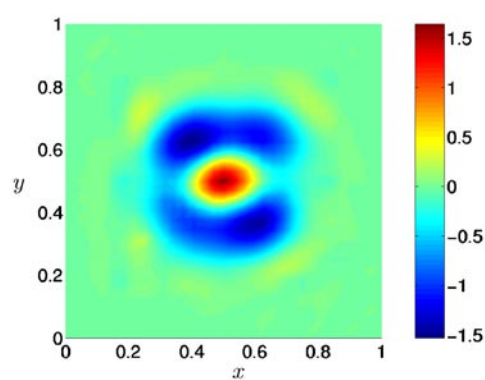
## 5.2. Noisy data

To test the performance of our imaging algorithm for noisy data, we add random, Gaussian, multiplicative noise to  $V_j$ , for  $j = 1, \dots, 27$ . First, we take a 2.5% noise level and obtain the image shown in figures 15 and 16. This reconstruction is done with a regularization parameter  $\alpha_2 = 5 \times 10^{-10}$ . For the reconstructed image, boundary misfit  $\sum_{j=1}^{27} \|\phi_j|_{\partial G_2} - V_j\|_2^2$  is at the noise level. Note that the image  $\rho^{(2)}$  is very close to the noiseless one shown in figures 11–14. The same is true for the coarse- and intermediate-grid images.

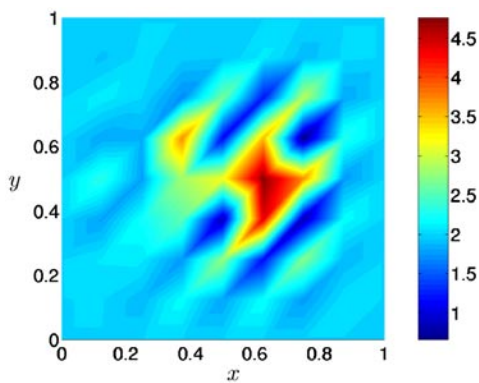
The good quality of the coarse-grid image in the experiments shown so far might lead us to the question: why bother to calculate  $\rho^{(2)}$  with the multigrid and not stop at  $\rho^{(0)}$ ? The advantage of doing fine-grid reconstruction is shown in the next experiment, where the noise level is 4.5%. The coarse-grid image shown in figures 17 and 18 is not as good as before and the smaller conductive region is misplaced. Nevertheless, this is corrected in the fine-grid



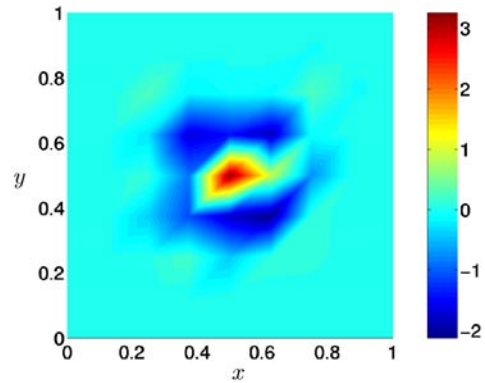
**Figure 15.** Real part of fine-grid image  $\rho^{(2)}$ . Noise level = 2.5%.



**Figure 16.** Imaginary part of fine-grid image  $\rho^{(2)}$ . Noise level = 2.5%.



**Figure 17.** Real part of coarse-grid image  $\rho^{(0)}$ . Noise level = 4.5%.



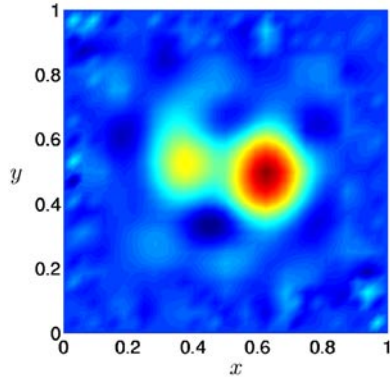
**Figure 18.** Imaginary part of coarse grid image  $\rho^{(0)}$ . Noise level = 4.5%.

image shown in figures 19 and 20. The regularization parameter on  $G_2$  is  $\alpha_2 = 10^{-9}$  and, at the end, the boundary misfit  $\sum_{j=1}^{27} \|\phi_j|_{\partial G_2} - V_j\|_2^2$  is at the noise level. Clearly, the images in figures 19 and 20 are not as good as the noiseless ones, but we can still distinguish the important features of the true admittivity. Moreover, the recovered image has a magnitude that remains close to the actual value of the true admittivity in  $\Omega$ .

### 5.3. Summary of numerical results

The numerical experiments presented in this section demonstrate that the nonlinear, nested iteration, multigrid algorithm (3.12) can be effective in inversion. The constructed images of admittivity function  $\rho$  have the correct geometrical features as well as a good contrast. Moreover, the algorithm is stable in the presence of noisy data. A key part in the success of the multigrid iteration is played by the coarse-grid solution. We have showed that algorithm (4.22), described in section 4.2, can give coarse-grid images  $\rho^{(0)}$  that are good approximations of the true admittivity. This is of great importance in the multigrid iteration (3.12) for two reasons:

- (1) We have a good starting admittivity in the nested iteration or, equivalently, a small starting residual. For example, in the case of noiseless data, before having the coarse-grid image,



**Figure 19.** Real part of fine-grid image  $\rho^{(2)}$ . Noise level = 4.5%.

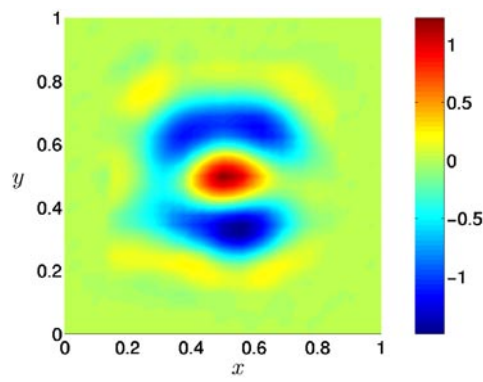


**Figure 20.** Imaginary part of fine-grid image  $\rho^{(2)}$ . Noise level = 4.5%.

the residual is  $5.0734578 \times 10^{-2}$ . After the coarse-grid solutions, the residual on  $G_2$  drops by two orders of magnitude.

(2) The coarse-grid corrections are effective in speeding up convergence.

The combination of these two attributes allows us to construct fine-grid images with just three calls of multigrid procedure **NMG**, on grid  $G_2$ , where computations are expensive.

In contrast, if the ideas of section 4 are not used in the coarse-grid calculations, we have found that, to get multigrid convergence, we need large regularization parameters. This is clearly undesirable because the images have poor resolution.

## 6. Convergence analysis

In this section, we establish the local convergence of the nonlinear multigrid algorithm (3.12), for the complex Dirichlet problem (2.15) and (3.1) written in abstract form as (3.2). To fix ideas, let us suppose that  $\Omega \subset \mathbb{R}^2$ . Our proof is based on the theory presented in [24] and it assumes that (3.2) is sufficiently regularized to achieve local convergence.

### 6.1. Definitions and regularity estimates

We proceed as in section 3.2 and write (3.2) or, equivalently, (2.15), (3.1), in the real form

$$\mathcal{L}(\alpha, u) = 0, \quad (6.1)$$

for some regularization parameter  $\alpha$ . For given admittivity  $\rho$  (or  $u$ ), potentials  $\phi_j$  and  $\psi_j$  entering the nonlinear part of equation (6.1) are solutions of (2.9) and (2.14), respectively. Suppose that in (2.9) and (2.14) we have a  $\rho \in H^2(\Omega)$ , with strictly positive real part. By Sobolev inequalities [32],  $\nabla \rho \in L_q(\Omega)$ , for any  $2 \leq q < \infty$  and, given a smooth boundary  $\partial\Omega$  and an excitation current  $I_j \in H^{\frac{1}{2}}(\partial\Omega)$ , equation (2.9) has a unique solution  $\phi_j \in H^2(\Omega)$  (see lemma 9.1 in [31]). Similarly, equation (2.14) has a unique solution  $\psi_j \in H^2(\Omega)$ . Hence, by Sobolev inequalities [32],  $\nabla \phi_j$  and  $\nabla \psi_j$  are in  $L_4(\Omega)$  and  $\nabla \overline{\phi_j} \cdot \nabla \psi_j \in L^2(\Omega)$ . In light of this result, we suppose that equation (6.1) has a solution  $u$ , or equivalently,  $\rho$  with  $\Delta \rho \in L_2(\Omega)$ . Given that such a solution  $\rho \in H^2(\Omega)$  exists, we show that the multigrid algorithm proposed in this paper is locally convergent. In what follows, we shall need the divided difference  $\mathcal{D}\mathcal{L}$  defined as

$$\mathcal{L}(\alpha, u + \delta u) - \mathcal{L}(\alpha, u) = \mathcal{D}\mathcal{L}(u, \delta u)\delta u, \quad (6.2)$$

where  $\alpha$  is fixed. To calculate  $\mathcal{DL}$ , we solve for  $\phi_j + \delta\phi_j$  and  $\psi_j + \delta\psi_j$  equations such as (2.9) and (2.14), with a perturbed admittivity  $\rho + \delta\rho$ , where the real and imaginary parts of  $\delta\rho$  are contained in  $\delta u$ . By arguments similar to the above, given  $\delta\rho \in H^2(\Omega)$ , we have that  $\delta\phi_j$  and  $\delta\psi_j \in H^2(\Omega)$  and so  $\mathcal{DL}(u, \delta u)\delta u \in L^2(\Omega)$ .

On grid  $G_l, l = 0, \dots, K$ , the discretization of (6.1) is

$$\mathcal{L}_l(\mathbf{u}_l) = \mathbf{0}, \tag{6.3}$$

where the regularization parameter is  $\alpha_l$ . Since our discretization is consistent, if (6.1) has a solution  $u \in H^2(\Omega)$ , we can suppose that (6.3) has a solution  $\mathbf{u}_l^*$  with bounded discrete  $H^2$  norm. To calculate  $\mathbf{u}_l^*$  with multigrid algorithms (3.16) and (3.17), we solve on coarser grids  $G_0, \dots, G_{l-1}$  equations such as (6.3), with a nonzero right-hand side. Therefore, we embed (6.3) into the family of equations

$$\mathcal{L}_l(\mathbf{u}_l) = \mathbf{g}_l. \tag{6.4}$$

Let  $L'_l \mathbf{u}_l$  be the discretization of the principal part  $-\alpha_l \Delta u$  of  $\mathcal{L}_l(\mathbf{u}_l)$ , such that

$$\mathcal{L}_l(\mathbf{u}_l) = L'_l \mathbf{u}_l + \mathcal{L}''_l(\mathbf{u}_l). \tag{6.5}$$

The divided difference  $\mathcal{DL}_l$  is given by

$$\mathcal{DL}_l(\mathbf{u}_l, \delta \mathbf{u}_l) = L'_l + \mathcal{DL}''_l(\mathbf{u}_l, \delta \mathbf{u}_l) \tag{6.6}$$

and, to simplify notation, we shall denote by  $L''_l$  the divided difference  $\mathcal{DL}''_l(\mathbf{u}_l, \delta \mathbf{u}_l)$  and by  $L_l$  the divided difference  $\mathcal{DL}_l(\mathbf{u}_l, \delta \mathbf{u}_l)$ , for  $\mathbf{u}_l$  and  $\mathbf{u}_l + \delta \mathbf{u}_l$  in a neighbourhood  $\mathcal{U}_l$  of the solution  $\mathbf{u}_l^*$ .

**Lemma 5.** *Suppose that admittivity  $\rho^{(l)}$  lies in  $\Upsilon$ . There exists an  $s > 0$  such that, for  $\alpha_l \geq O(h_l^s)$ ,*

$$\lim_{h_l \rightarrow 0} \frac{h_l^2}{\alpha_l} \|L''_l\|_{h_l,0 \leftarrow h_l,2} = \lim_{h_l \rightarrow 0} \frac{h_l^2}{\alpha_l} \|L''_l\|_{h_l,0 \leftarrow h_l,1} = \lim_{h_l \rightarrow 0} \frac{h_l^2}{\alpha_l} \|L''_l\|_{h_l,0 \leftarrow h_l,0} = 0 \tag{6.7}$$

and, in fact,

$$\frac{h_l^2}{\alpha_l} L''_l = O(h_l^s). \tag{6.8}$$

Here, we take the discrete norms

$$\begin{aligned} \|L''_l\|_{h_l,0 \leftarrow h_l,2} &= \sup_{\mathbf{u}_l \neq \mathbf{0}} \frac{\|L''_l \mathbf{u}_l\|_{h_l,0}}{\|\mathbf{u}_l\|_{h_l,2}}, \\ \|L''_l\|_{h_l,0 \leftarrow h_l,1} &= \sup_{\mathbf{u}_l \neq \mathbf{0}} \frac{\|L''_l \mathbf{u}_l\|_{h_l,0}}{\|\mathbf{u}_l\|_{h_l,1}}, \\ \|L''_l\|_{h_l,0 \leftarrow h_l,0} &= \sup_{\mathbf{u}_l \neq \mathbf{0}} \frac{\|L''_l \mathbf{u}_l\|_{h_l,0}}{\|\mathbf{u}_l\|_{h_l,0}}, \\ \|\mathbf{u}_l\|_{h_l,2} &= \left[ \|\mathbf{u}_l\|_{h_l,0}^2 + \|\nabla_{h_l} \mathbf{u}_l\|_{h_l,0}^2 + \sum_{i,j=1}^2 \|\partial_{i,h_l} \partial_{j,h_l} \mathbf{u}_l\|_{h_l,0}^2 \right]^{\frac{1}{2}}, \\ \|\mathbf{u}_l\|_{h_l,1} &= \left[ \|\mathbf{u}_l\|_{h_l,0}^2 + \|\nabla_{h_l} \mathbf{u}_l\|_{h_l,0}^2 \right]^{\frac{1}{2}}, \\ \|\mathbf{u}_l\|_{h_l,0} &= \left[ h_l^2 \sum_{\mathbf{x} \in G_l} |\mathbf{u}_l(\mathbf{x})|^2 \right]^{\frac{1}{2}}, \end{aligned} \tag{6.9}$$

where  $\partial_{i,h_l}$  and  $\nabla_{h_l} \mathbf{u}_l$  are finite-difference derivatives in the  $i$ th direction and gradients, respectively.

**Proof.** Consider on grid  $G_l$  an admittivity  $\rho^{(l)}$  which is bounded and has positive real part. In our algorithm, we calculate potentials  $\phi_j$  and  $\psi_j$  by solving equations (2.9) and (2.14), where the admittivity is approximated by  $r^{(l)}(\mathbf{x}) = \mathcal{P}\rho^{(l)}(\mathbf{x})$ , the piecewise linear interpolation of  $\rho^{(l)}$ . We denote these potentials by  $\phi_j(\mathbf{x}; r^{(l)})$  and  $\psi_j(\mathbf{x}; r^{(l)})$ , respectively, and, since  $r^{(l)} \in C^0(\overline{\Omega})$ , theorem 3.8 in [25] gives that  $\phi_j$  and  $\psi_j$  are Hölder continuous, with Hölder coefficient  $0 < \beta < 1$ , but arbitrarily close to one.

Numerical approximations  $\phi_j^{(l)}$  and  $\psi_j^{(l)}$  of potentials  $\phi_j(\mathbf{x}; r^{(l)})$  and  $\psi_j(\mathbf{x}; r^{(l)})$  are calculated with a piecewise linear finite-element method and the following  $L^\infty$  error estimates [6] hold. There exists a finite  $C > 0$  such that  $\lim_{h_l \rightarrow 0} \|\phi_j - \phi_j^{(l)}\|_{L^\infty(\Omega)} \leq C \lim_{h_l \rightarrow 0} h_l^\beta |\log h_l| = 0$  and, similarly,  $\lim_{h_l \rightarrow 0} \|\psi_j - \psi_j^{(l)}\|_{L^\infty(\Omega)} \leq C \lim_{h_l \rightarrow 0} h_l^\beta |\log h_l| = 0$ . Therefore, for arbitrary grid points  $\mathbf{x}$  and  $\mathbf{y}$ , satisfying  $|\mathbf{x} - \mathbf{y}| = O(h_l)$ , we can find a positive  $s < \beta$  that gives

$$|\phi_j^{(l)}(\mathbf{x}) - \phi_j^{(l)}(\mathbf{y})| = O(h_l^s) \text{ and } |\psi_j^{(l)}(\mathbf{x}) - \psi_j^{(l)}(\mathbf{y})| = O(h_l^s), \tag{6.10}$$

uniformly in  $G_l$ .

By the same argument, given a bounded perturbation  $\delta\rho^{(l)}$  (or  $\delta\mathbf{u}_l$ ) of the admittivity on  $G_l$ , we find that perturbations  $\delta\phi_j^{(l)}$  and  $\delta\psi_j^{(l)}$  of the potentials satisfy equations similar to (6.10). The entries in  $\{L_l''\}\delta\mathbf{u}_l$  are given by

$$\sum_{p=1}^{N_{\text{exp}}} [\nabla_{h_l} \delta\bar{\phi}_p^{(l)}(\mathbf{x}_i) \cdot \nabla_{h_l} \psi_p^{(l)}(\mathbf{x}_i) + \nabla_{h_l} \bar{\phi}_p^{(l)}(\mathbf{x}_i) \cdot \nabla_{h_l} \delta\psi_p^{(l)}(\mathbf{x}_i)], \tag{6.11}$$

where  $\nabla_{h_l}$  is the discrete gradient calculated with second-order finite differences. In light of (6.10), for sufficiently small  $h_l$ , all discrete gradients in (6.11) are  $O(\frac{h_l^s}{h_l})$  and, given  $\alpha_l \geq O(h_l^s)$ , all entries in  $\frac{h_l^2}{\alpha_l} L_l''$  are  $O(h_l^s)$  and lemma 5 is proved.  $\square$

Note that, at fixed  $h_l$ ,  $r^{(l)}(\mathbf{x}) = \mathcal{P}\rho^{(l)}(\mathbf{x})$  has its gradient in  $L^p(\overline{\Omega})$ , for  $p > 2$ . Therefore, for smooth  $\partial\Omega$  and  $I_j \in H^{\frac{1}{2}}(\partial\Omega)$ , lemma 9.1 in [31] gives that potentials  $\phi_j(\mathbf{x}; r^{(l)})$  and  $\psi_j(\mathbf{x}; r^{(l)})$  are in  $H^2(\Omega)$ . Similarly, the gradient of  $\delta r^{(l)}(\mathbf{x}) = \mathcal{P}\delta\rho^{(l)}(\mathbf{x})$  is in  $L^p(\Omega)$ , for  $p > 2$ , so perturbations  $\delta\phi_j(\mathbf{x}; r^{(l)})$  and  $\delta\psi_j(\mathbf{x}; r^{(l)})$  are functions in  $H^2(\Omega)$  and, by Sobolev inequalities [32],  $\nabla\delta\bar{\phi}_j \cdot \nabla\psi_j + \nabla\bar{\phi}_j \cdot \nabla\delta\psi_j \in L^2(\Omega)$ . We approximate  $\phi_j(\mathbf{x}; r^{(l)})$ ,  $\psi_j(\mathbf{x}; r^{(l)})$ ,  $\delta\phi_j(\mathbf{x}; r^{(l)})$  and  $\delta\psi_j(\mathbf{x}; r^{(l)})$  by the finite-element solutions  $\phi_j^{(l)}$ ,  $\psi_j^{(l)}$ ,  $\delta\phi_j^{(l)}$  and  $\delta\psi_j^{(l)}$ , respectively, so we can suppose that  $\|\nabla_{h_l} \delta\bar{\phi}_j \cdot \nabla_{h_l} \psi_j + \nabla_{h_l} \bar{\phi}_j \cdot \nabla_{h_l} \delta\psi_j\|_{h_l,0}$  is finite. Finally, given definition (6.11) of the entries in  $L_l''\delta\mathbf{u}_l$ ,  $\|L_l''\delta\mathbf{u}_l\|_{h_l,0} \leq C$  and, in fact,

$$\|L_l''\|_{h_l,0 \leftarrow h_l,2} \leq C. \tag{6.12}$$

For  $L_l$ , we have the discrete two-regularity estimate.

**Lemma 6.** *There exists an  $s > 0$  such that, for  $\alpha_l \geq O(h_l^s)$  and a sufficiently small, but finite, mesh size  $h_l$ , we have*

$$\|L_l^{-1}\mathbf{g}_l\|_{h_l,2} \leq \frac{C}{\alpha_l} \|\mathbf{g}_l\|_{h_l,0}, \tag{6.13}$$

where  $C$  is a finite, positive constant.

**Proof.** It is known [42] that the principal part of  $L_l$  satisfies

$$\|(L_l')^{-1}\mathbf{g}_l\|_{h_l,2} \leq \frac{C'}{\alpha_l} \|\mathbf{g}_l\|_{h_l,0}, \tag{6.14}$$

for some finite, positive constant  $C'$ . Since  $L'_l$  is of order  $\frac{\alpha_l}{h_l^2}$ ,

$$L_l = [I_l + L''_l(L'_l)^{-1}]L'_l = \left[ I_l + O\left(\frac{h_l^2}{\alpha_l}\right) L''_l \right] L'_l, \quad (6.15)$$

where  $I_l$  is the identity matrix in  $\mathbb{R}^{2(n_l-1)^2}$ . By lemma 5,  $\frac{h_l^2}{\alpha_l} L''_l = O(h_l^s)$  and, for sufficiently small  $h_l$ ,

$$\|[I_l + L''_l(L'_l)^{-1}]^{-1}\|_{h_l,0 \leftarrow h_l,0} \leq C''. \quad (6.16)$$

Inequalities (6.14) and (6.16) give

$$\begin{aligned} \|(L_l)^{-1} \mathbf{g}_l\|_{h_l,2} &= \|(L'_l)^{-1} [I_l + L''_l(L'_l)^{-1}]^{-1} \mathbf{g}_l\|_{h_l,2} \\ &\leq \frac{C'}{\alpha_l} \|[I_l + L''_l(L'_l)^{-1}]^{-1} \mathbf{g}_l\|_{h_l,0} \leq \frac{C' C''}{\alpha_l} \|\mathbf{g}_l\|_{h_l,0}, \end{aligned} \quad (6.17)$$

and (6.13) follows.  $\square$

**Lemma 7.** *At the solution  $\mathbf{u}_l^*$ ,  $\mathcal{L}_l$  is continuous.*

**Proof.** By assumption,  $\mathbf{u}_l^* \in H^2(\Omega)$  and we define a neighbourhood  $\mathcal{U}_l$  of  $\mathbf{u}_l^*$ , where  $\|\mathbf{u}_l - \mathbf{u}_l^*\|_{h_l,2}$  is bounded. Given  $\mathbf{u}_l \in \mathcal{U}_l$  and inequality (6.16), we have

$$\begin{aligned} \|\mathcal{L}_l(\mathbf{u}_l) - \mathcal{L}_l(\mathbf{u}_l^*)\|_{h_l,0} &= \|(L'_l + L''_l)(\mathbf{u}_l - \mathbf{u}_l^*)\|_{h_l,0} = \|[I_l + L''_l(L'_l)^{-1}]L'_l(\mathbf{u}_l - \mathbf{u}_l^*)\|_{h_l,0} \\ &\leq C'' \|L'_l(\mathbf{u}_l - \mathbf{u}_l^*)\|_{h_l,0} \leq C'' \alpha_l \|\mathbf{u}_l - \mathbf{u}_l^*\|_{h_l,2} \end{aligned} \quad (6.18)$$

and so  $\mathcal{L}_l$  is continuous.

By lemmas 5 and 6,  $L_l$  exists, is invertible and satisfies the discrete two-regularity (6.13). Furthermore, potentials  $\phi_j$ ,  $\psi_j$  and their perturbations  $\delta\phi_j$  and  $\delta\psi_j$  vary continuously with the admittivity (see [14]), so  $L_l$  is continuous in  $\rho^{(l)}$ , as well. Finally, by lemma 7,  $\mathcal{L}_l$  is continuous at the solution. Therefore, the implicit function theorem [36] gives that there exists a neighbourhood  $\mathcal{U}_l \subset \mathbb{R}^{2(n_l-1)^2}$  of  $\mathbf{u}_l^*$ , connected to a neighbourhood of  $\mathbf{0}$ , say  $\mathcal{G}_l \subset \mathbb{R}^{2(n_l-1)^2}$ , such that  $\mathcal{L}_l : \mathcal{U}_l \rightarrow \mathcal{G}_l$  is a bijection and  $\mathcal{L}_l$  and  $\mathcal{L}_l^{-1}$  are continuous. Hence, for  $\mathbf{g}_l \in \mathcal{G}_l$ , (6.4) is well defined and we can write its solution as  $\mathcal{L}_l^{-1}(\mathbf{g}_l)$ .  $\square$

## 6.2. Convergence

In (3.12), let  $j = 1, \dots, \tilde{M}$ , denote the iteration number at level  $l$ , such that

$$\mathbf{u}_l^{j+1} \leftarrow \mathbf{NMG M}(l, \mathbf{u}_l^j, \mathbf{0}), \quad (6.19)$$

where  $\mathbf{NMG M}$  is defined either by (3.17) or (3.16). We show that this iteration is a contraction, provided that the coarse-grid solutions are sufficiently accurate and  $\mathcal{L}_l$  is regularized appropriately.

**Theorem 6.1.** *Suppose that  $\mathbf{u}_k$  are sufficiently close to  $\mathbf{u}_k^* = \mathcal{L}_k^{-1}(\mathbf{0})$ , for  $k = 0, 1, \dots, l-1$  and  $\mathbf{g}_l \in \mathcal{G}_l$ . For a sufficiently large regularization parameter  $\alpha_l$ , nonlinear multigrid iterations (3.17) or (3.16) give*

$$\|\mathbf{u}_l^{j+1} - \mathcal{L}_l^{-1}(\mathbf{g}_l)\|_{h_l,0} \leq \xi_l \|\mathbf{u}_l^j - \mathcal{L}_l^{-1}(\mathbf{g}_l)\|_{h_l,0}, \quad \xi_l < 1, \quad (6.20)$$

where  $j$  stands for iteration and  $\xi_l$  is the contraction number.

The nonlinear nested iteration (3.12) makes  $\tilde{M}$  calls of procedure **NMGM**, on each grid level. The initial guess on  $G_l$ ,  $\mathbf{u}_l^0$ , is the interpolation of the solution on coarser grid  $G_{l-1}$ . Given that **NMGM** is a contraction, the convergence of nonlinear nested iteration (3.12) depends on the consistency condition [24]

$$\|\mathcal{P}\mathbf{u}_{l-1}^* - \mathbf{u}_l^*\|_{h_l,0} \leq C_1 h_l^\kappa, \quad l = 1, 2, \dots, K, \tag{6.21}$$

that the solutions of (6.3) on  $G_l$  and  $G_{l-1}$  must satisfy, for some  $\kappa > 0$ . We have a consistent discretization (6.3) of equation (6.1), as described in section 3.1. The nine point discretization  $L_l' \mathbf{u}_l$  of the principal part of  $\mathcal{L}_l(\mathbf{u}_l)$  is second-order accurate. The nonlinear part  $\mathcal{L}_l''(\mathbf{u}_l)$  involves gradients of the electric and adjoint potentials  $\phi_k$  and  $\psi_k$ , for  $k = 1, \dots, N_{\text{exp}}$ . Since we calculate these potentials with a piecewise linear finite-element scheme,  $\nabla \bar{\phi}_k \cdot \nabla \psi_k$  is first-order accurate and so is  $\mathcal{L}_l''(\mathbf{u}_l)$ . Therefore, we expect (6.21) to hold with  $\kappa = 1$ . We have the following convergence result.

**Theorem 6.2.** *Assume that  $h_l$  is small enough to have  $C_1 h_l^\kappa \leq \epsilon_l$  or, equivalently,  $\mathcal{P}\mathbf{u}_{l-1}^* \in \mathcal{U}_l$ , for all grid levels  $l = 1, 2, \dots, K$ , and also assume that the regularization parameter  $\alpha_l$  is sufficiently large. Let  $C_2$  be defined as the upper bound  $\|\mathcal{P}\|_{h_l,0 \leftarrow h_l,0} \leq C_2$  and suppose that the coarse-grid solution  $\mathbf{u}_0$  in (3.12) has finite  $\|\cdot\|_{h_0,2}$  norm and it satisfies*

$$\|\mathbf{u}_0 - \mathbf{u}_0^*\|_{h_0,0} \leq C h_0^\kappa. \tag{6.22}$$

The nonlinear nested iteration (3.12) is well defined and

$$\|\mathbf{u}_K - \mathbf{u}_K^*\|_{h_K,0} \leq C_1 \frac{\xi^{\tilde{M}}}{1 - 2C_2 \xi^{\tilde{M}}} h_K^\kappa, \tag{6.23}$$

where  $\tilde{M}$  is the number of calls of procedure **NMGM**,  $\xi = \sup_{l=1,\dots,K} \xi_l$  and  $\xi_l$  is the contraction number in theorem 6.1.

Note that, for the nine-point interpolation  $\mathcal{P}$  defined in section 3.1,  $C_2$  is finite. Moreover, in (6.23), we assume that number  $\tilde{M}$  of calls of procedure **NMGM** is large enough to have  $2C_2 \xi^{\tilde{M}} < 1$ . Finally, note that theorem 6.2 assumes an accurate coarse-grid solution, so we have just local convergence.

A successful multigrid algorithm combines a relaxation scheme, that smoothes the error, with a coarse-grid correction. A natural measure of smoothness of the error  $\delta \mathbf{u}_l = \mathbf{u}_l - \mathbf{u}_l^*$  is some norm of divided differences of  $\delta \mathbf{u}_l$ . In particular, we can use the second-order difference operator given by the Jacobian  $L_l$ . Then, the smoothing number on  $G_l$  can be defined as  $\eta_l(v) = \frac{\|L_l S_l^{(v)}\|_{h_l,0 \leftarrow h_l,0}}{\|L_l\|_{h_l,0 \leftarrow h_l,0}}$ , where  $\eta_l(v) \geq 1$  indicates no smoothing. In section 6.2.2, we show that there exists an  $s > 0$  such that, given a regularization parameter  $\alpha_l \geq O(h_l^s)$ , the relaxation scheme (3.14) satisfies the *smoothing property*

$$\|L_l S_l^{(v)}\|_{h_l,0 \leftarrow h_l,0} \leq \eta_l(v) \frac{\alpha_l}{h_l^2}, \tag{6.24}$$

where smoothing number  $\eta_l(v) \rightarrow 0$ , as the number of relaxation sweeps  $v$  tends to infinity.

The second key component of the multigrid algorithm is the coarse-grid correction. Given that the error on  $G_l$  is smooth, a successful coarse-grid correction requires that the linearization of (6.3) satisfies the approximation property

$$\|L_l^{-1} - \mathcal{P}L_{l-1}^{-1}\mathcal{R}\|_{h_l,0 \leftarrow h_l,0} \leq C_A \frac{h_l^2}{\alpha_l}, \tag{6.25}$$

where  $C_A$  is some finite, positive constant. Inequality (6.25) is proved in section 6.2.3.

Finally, in section 6.2.1, we prove that the nonlinear multigrid iterations are well defined. That is, at all steps,  $\mathbf{u}_l \in \mathcal{U}_l$  and  $\mathbf{g}_l \in \mathcal{G}_l$ , for  $l = 0, 1, \dots, K$ . Then, theorems 6.1 and 6.2 follow from the known nonlinear multigrid convergence results in theorems 9.5.12 and 9.5.13 of [24].

6.2.1. *Proof that iterations are well defined.* In this section, we show that **NMGM** given by either (3.16) or (3.17) is well defined. Let us define a  $2(n_l - 1)^2$ -dimensional ball

$$\mathcal{B}U_l(\epsilon) = \{\mathbf{u}_l \in \mathbb{R}^{2(n_l-1)^2} \text{ such that } \|\mathbf{u}_l - \mathbf{u}_l^*\|_{h_l,2} \leq \epsilon\}, \quad (6.26)$$

and denote by  $\epsilon_l$  the radius of the largest ball in  $\mathcal{U}_l$ . The image of  $\mathcal{B}U_l(\epsilon)$ , through bijection  $\mathcal{L}_l$ , is named  $\mathcal{B}G_l(\epsilon)$ . For nonlinear multigrid procedure **NMGM** given by (3.17), we have the following.

**Lemma 8.** *In (3.17), assume that  $\mathbf{u}_{l-1} \in \mathcal{B}U_{l-1}(\frac{\epsilon_{l-1}}{2})$ . There exists a  $\tau$  such that  $\mathbf{d}$  belongs to  $\mathcal{B}G_{l-1}(\epsilon_{l-1})$ .*

**Proof.** This proof is basically the same as that given in [24]. For completeness, we prefer to present it here, as well. From (3.17),

$$\mathbf{d} = \mathbf{g}_{l-1} + \tau \mathcal{R}[\mathbf{g}_l - \mathcal{L}_l(\mathbf{u}_l)], \quad (6.27)$$

and we must show that

$$\|\mathcal{L}_{l-1}^{-1}(\mathbf{d}) - \mathbf{u}_{l-1}^*\|_{h_{l-1},2} \leq \epsilon_{l-1}. \quad (6.28)$$

We have the divided differences

$$\begin{aligned} \mathcal{L}_l(\mathbf{u}_l) - \mathcal{L}_l(\tilde{\mathbf{u}}_l) &= \mathcal{D}\mathcal{L}_l(\mathbf{u}_l, \tilde{\mathbf{u}}_l)(\mathbf{u}_l - \tilde{\mathbf{u}}_l), & \text{for all } \mathbf{u}_l, \tilde{\mathbf{u}}_l \in \mathcal{U}_l, \\ \mathcal{L}_l^{-1}(\mathbf{g}_l) - \mathcal{L}_l^{-1}(\tilde{\mathbf{g}}_l) &= \mathcal{D}\mathcal{L}_l^{-1}(\mathcal{L}_l^{-1}(\mathbf{g}_l), \mathcal{L}_l^{-1}(\tilde{\mathbf{g}}_l))(\mathbf{g}_l - \tilde{\mathbf{g}}_l), & \text{for all } \mathbf{g}_l, \tilde{\mathbf{g}}_l \in \mathcal{G}_l, \end{aligned} \quad (6.29)$$

where  $\mathcal{D}\mathcal{L}_l^{-1}(\mathbf{u}_l, \tilde{\mathbf{u}}_l) = [\mathcal{D}\mathcal{L}_l(\mathbf{u}_l, \tilde{\mathbf{u}}_l)]^{-1}$ . By definition (6.27) and  $\mathbf{u}_{l-1} = \mathcal{L}_{l-1}^{-1}(\mathbf{g}_{l-1})$ , we have

$$\mathcal{L}_{l-1}^{-1}(\mathbf{d}) - \mathbf{u}_{l-1} = \tau [\mathcal{D}\mathcal{L}_{l-1}(\mathbf{u}_{l-1}, \mathcal{L}_{l-1}^{-1}(\mathbf{d}))]^{-1} \mathcal{R}[\mathbf{g}_l - \mathcal{L}_l(\mathbf{u}_l)]. \quad (6.30)$$

From lemma 6 we can infer that there exists a finite constant  $C_L$  such that

$$\|[\mathcal{D}\mathcal{L}_{l-1}(\mathbf{u}_{l-1}, \tilde{\mathbf{u}}_{l-1})]^{-1}\|_{h_{l-1},2 \leftarrow h_{l-1},0} \leq C_L, \quad \text{for all } \mathbf{u}_{l-1}, \tilde{\mathbf{u}}_{l-1} \in \mathcal{U}_{l-1}, \quad (6.31)$$

and we define  $\tau$  as [24]

$$\frac{1}{\tau} = \frac{2C_L}{\epsilon_{l-1}} \|\mathcal{R}[\mathbf{g}_l - \mathcal{L}_l(\mathbf{u}_l)]\|_{h_{l-1},0}. \quad (6.32)$$

Note that, in (6.32), we assume that equation (6.4) on grid  $G_l$  is not solved, yet, so  $\mathbf{g}_l - \mathcal{L}_l(\mathbf{u}_l) \neq 0$ . Moreover, the right-hand side of (6.32) is bounded, as follows from  $\|\mathbf{u}_l\|_{h_l,2} \leq C$  and  $\|\mathcal{L}_l''\|_{h_l,0} \leq C'$ . The proof of lemma 8 is now complete because (6.32) gives

$$\|\mathcal{L}_{l-1}^{-1}(\mathbf{d}) - \mathbf{u}_{l-1}^*\|_{h_{l-1},2} \leq \|\mathcal{L}_{l-1}^{-1}(\mathbf{d}) - \mathbf{u}_{l-1}\|_{h_{l-1},2} + \|\mathbf{u}_{l-1} - \mathbf{u}_{l-1}^*\|_{h_{l-1},1} \leq \frac{\epsilon_{l-1}}{2} + \frac{\epsilon_{l-1}}{2}. \quad (6.33)$$

Definition (6.32) is difficult to apply in practice, because we do not know the bound  $C_L$ . In our numerical experiments, choice  $\tau = 0.1$  proved successful. The FAS algorithm (3.16) does not require such a parameter but it has the disadvantage that, in general, one cannot guarantee that  $\mathbf{d}$  belongs to  $\mathcal{G}_{l-1}$ . In all our numerical experiments, we achieved  $\mathbf{d} \in \mathcal{G}_{l-1}$  for properly chosen regularization parameters  $\alpha_l$ . For the analysis of (3.16), see [24].  $\square$

6.2.2. *The smoothing property.* For relaxation (3.14), let us define divided differences  $\mathcal{D}S_l^{(v)}$ , where

$$S_l^{(v)}(\mathbf{u}_l, \mathbf{g}_l) - S_l^{(v)}(\tilde{\mathbf{u}}_l, \mathbf{g}_l) = \mathcal{D}S_l^{(v)}(\mathbf{u}_l, \tilde{\mathbf{u}}_l, \mathbf{g}_l)(\mathbf{u}_l - \tilde{\mathbf{u}}_l), \tag{6.34}$$

and  $S_l(\mathbf{u}_l, \mathbf{u}_l, \mathbf{g}_l) = \mathcal{D}S_l^{(v)}(\mathbf{u}_l, \mathbf{u}_l, \mathbf{g}_l)$ . Moreover, let us write  $S_l = S'_l + S''_l$ , where  $S'_l$  stands for relaxation of the linear, principal part  $L'_l$  of  $\mathcal{L}_l$ . In this section, we prove the smoothing property for  $L_l$  and  $S_l$ .

**Lemma 9.** *There exists an  $s > 0$  such that, for  $\alpha_l \geq O(h_l^s)$ , we have the smoothing property*

$$\|L_l S_l^{(v)}\|_{h_l,0 \leftarrow h_l,0} \leq \eta_l(v) \frac{\alpha_l}{h_l^2}, \quad \text{for } 1 \leq v \leq \bar{v}(h_l), \tag{6.35}$$

where  $\lim_{v \rightarrow \infty} \eta_l(v) = 0$  and  $\lim_{h_l \rightarrow 0} \bar{v}(h_l) = \infty$ . Moreover, there exists a finite  $C_S(v)$  such that

$$\|S_l^{(v)}\|_{h_l,0 \leftarrow h_l,0} \leq C_S(v), \quad \text{for all } 1 \leq v \leq \bar{v}(h_l). \tag{6.36}$$

**Proof.** To prove lemma 9, we use criterion 6.2.7 in [24], which states that (6.35) and (6.36) hold, provided

$$\begin{aligned} \|L'_l S_l^{(v)}\|_{h_l,0 \leftarrow h_l,0} &\leq \eta'_l(v) \frac{\alpha_l}{h_l^2}, \quad \text{for } 1 \leq v \leq \bar{v}'(h_l), \\ \text{where } \lim_{v \rightarrow \infty} \eta'_l(v) &= 0, \quad \lim_{h_l \rightarrow 0} \bar{v}'(h_l) = \infty, \end{aligned} \tag{6.37}$$

$$\|S_l^{(v)}\|_{h_l,0 \leftarrow h_l,0} \leq C'_S(v), \tag{6.38}$$

$$\lim_{h_l \rightarrow 0} \|S_l^{(v)}\|_{h_l,0 \leftarrow h_l,0} = 0, \quad \text{for all } 1 \leq v \leq \bar{v}'(h_l) \quad \text{and} \tag{6.39}$$

$$\lim_{h_l \rightarrow 0} \frac{h_l^2}{\alpha_l} \|L_l\|_{h_l,0 \leftarrow h_l,0} = 0. \tag{6.40}$$

Criterion 6.2.7 in [24] also gives that, in (6.35),  $\eta_l(v) = (1 + \delta)\eta'_l(v)$ , for some positive  $\delta$  and, in (6.36),  $C_S(v) = C'_S(v) + \text{constant}$ .

Limit (6.40) is already stated in lemma 5, so we concentrate on proving (6.37), (6.38) and (6.39). The relaxation scheme is block Gauss–Seidel, with one Newton step, as explained in section 3.2. After a proper ordering of the components of  $\mathbf{u}_l$ , we make the splitting

$$\begin{aligned} L'_l &= D'_l - A'_l - B'_l, \\ L''_l &= D''_l - A''_l - B''_l, \end{aligned} \tag{6.41}$$

where  $D'_l + D''_l$ ,  $A'_l + A''_l$  and  $B'_l + B''_l$  are block diagonal, lower and upper triangular parts of  $L_l$ , respectively. The relaxation matrices are

$$\begin{aligned} S_l &= (D'_l + D''_l - A'_l - A''_l)^{-1}(B'_l + B''_l), \\ S'_l &= (D'_l - A'_l)^{-1}B'_l, \\ S''_l &= \{[I_l + (D'_l - A'_l)^{-1}(D''_l - A''_l)]^{-1} - I_l\}S'_l \\ &\quad + [I_l + (D'_l - A'_l)^{-1}(D''_l - A''_l)]^{-1}(D'_l - A'_l)^{-1}B''_l. \end{aligned} \tag{6.42}$$

Clearly,  $S_l^{(v)} = (S'_l)^v$  and, as shown in [24], proposition 6.2.23, (6.38) is satisfied. Furthermore,  $L'_l$  is symmetric and positive definite with positive definite block diagonal  $D'_l$ , so Gauss–Seidel converges and it satisfies the smoothing property (6.37) (see note 6.2.19 [24]).

To prove (6.39), we use that  $L'_l$  and its lower triangular part  $D'_l - A'_l$  are  $O(\frac{\alpha_l}{h_l^2})$ . From lemma 5 we have that  $\frac{h_l^2}{\alpha_l} L''_l = O(h_l^s)$  and, by (6.41),  $\frac{h_l^2}{\alpha_l}(D''_l - A''_l)$  and  $\frac{h_l^2}{\alpha_l} B''_l$  are  $O(h_l^s)$ , as

well. Then, (6.42) gives

$$S_l'' = \left\{ \left[ I_l + O\left(\frac{h_l^2}{\alpha_l}\right)(D_l'' - A_l'') \right]^{-1} - I_l \right\} S_l' + \left[ I_l + O\left(\frac{h_l^2}{\alpha_l}\right)(D_l'' - A_l'') \right]^{-1} O\left(\frac{h_l^2}{\alpha_l}\right) B_l'' \rightarrow 0, \quad \text{as } h_l \rightarrow 0,$$

and (6.39) follows.  $\square$

**6.2.3. The approximation property.** In this section, we establish the approximation property for divided differences  $L_l$ .

**Lemma 10.** *There exists an  $s > 0$  such that, given  $\alpha_l \geq O(h_l^s)$ , the prolongation  $\mathcal{P}$  and restriction  $\mathcal{R}$  defined in section 3.1, we can find a finite positive  $C_A$  such that*

$$\|L_l^{-1} - \mathcal{P}L_{l-1}^{-1}\mathcal{R}\|_{h_l,0 \leftarrow h_{l-1},0} \leq C_A \frac{h_l^2}{\alpha_l}. \tag{6.43}$$

**Proof.** From (6.6), we have

$$\begin{aligned} L_l^{-1} &= (L_l')^{-1} [I_l + L_l''(L_l')^{-1}]^{-1}, \\ L_{l-1}^{-1} &= (L_{l-1}')^{-1} [I_{l-1} + L_{l-1}''(L_{l-1}')^{-1}]^{-1}, \end{aligned} \tag{6.44}$$

where  $I_l$  and  $I_{l-1}$  are identity matrices in  $\mathbb{R}^{2(m_l-1)^2}$  and  $\mathbb{R}^{2(m_{l-1}-1)^2}$ , respectively. Let us define

$$\begin{aligned} \Gamma_l &= [I_l + L_l''(L_l')^{-1}]^{-1} - I_l, \\ \Gamma_{l-1} &= [I_{l-1} + L_{l-1}''(L_{l-1}')^{-1}]^{-1} - I_{l-1}. \end{aligned} \tag{6.45}$$

Since  $(L_l')^{-1} = O(\frac{h_l^2}{\alpha_l})$ , by lemma 5,  $\Gamma_l$  in (6.45) is  $O(h_l^s)$ . Similarly,  $(L_{l-1}')^{-1} = O(\frac{h_{l-1}^2}{\alpha_{l-1}})$  and  $\Gamma_{l-1} = O(h_{l-1}^s)$ . Then,

$$\begin{aligned} \|L_l^{-1} - \mathcal{P}L_{l-1}^{-1}\mathcal{R}\|_{h_l,0 \leftarrow h_{l-1},0} &= \|(L_l')^{-1} - \mathcal{P}(L_{l-1}')^{-1}\mathcal{R} + (L_l')^{-1}\Gamma_l \\ &\quad - \mathcal{P}(L_{l-1}')^{-1}\Gamma_{l-1}\mathcal{R}\|_{h_l,0 \leftarrow h_{l-1},0} \leq \|(L_l')^{-1} - \mathcal{P}(L_{l-1}')^{-1}\mathcal{R}\|_{h_l,0 \leftarrow h_{l-1},0} \\ &\quad + \|(L_l')^{-1}\Gamma_l - \mathcal{P}(L_{l-1}')^{-1}\Gamma_{l-1}\mathcal{R}\|_{h_l,0 \leftarrow h_{l-1},0}. \end{aligned} \tag{6.46}$$

$L_l'$  is a second-order accurate discretization of  $-\alpha_l \Delta u$  and, from the known approximation property of the discrete Laplace operator [24], we obtain

$$\|(L_l')^{-1} - \mathcal{P}(L_{l-1}')^{-1}\mathcal{R}\|_{h_l,0 \leftarrow h_{l-1},0} \leq \frac{C'_A}{\alpha_l} h_l^2. \tag{6.47}$$

The second term in (6.46) can be bounded as

$$\begin{aligned} \|(L_l')^{-1}\Gamma_l - \mathcal{P}(L_{l-1}')^{-1}\Gamma_{l-1}\mathcal{R}\|_{h_l,0 \leftarrow h_{l-1},0} &\leq \|[(L_l')^{-1} - \mathcal{P}(L_{l-1}')^{-1}\mathcal{R}]\Gamma_l\|_{h_l,0 \leftarrow h_{l-1},0} \\ &\quad + \|\mathcal{P}(L_{l-1}')^{-1}(\mathcal{R}\Gamma_{l-1} - \Gamma_{l-1}\mathcal{R})\|_{h_l,0 \leftarrow h_{l-1},0}, \end{aligned} \tag{6.48}$$

and, from (6.47) and  $(L_l')^{-1} = O(\frac{h_l^2}{\alpha_l})$ , we have

$$\begin{aligned} \|(L_l')^{-1}\Gamma_l - \mathcal{P}(L_{l-1}')^{-1}\Gamma_{l-1}\mathcal{R}\|_{h_l,0 \leftarrow h_{l-1},0} &\leq C'_A \frac{h_l^2}{\alpha_l} \|\Gamma_l\|_{h_l,0 \leftarrow h_{l-1},0} \\ &\quad + \|\mathcal{P}\|_{h_l,0 \leftarrow h_{l-1},0} \|(L_{l-1}')^{-1}\|_{h_{l-1},0 \leftarrow h_{l-1},0} \|\mathcal{R}\Gamma_{l-1} - \Gamma_{l-1}\mathcal{R}\|_{h_{l-1},0 \leftarrow h_{l-1},0} \leq C \frac{h_l^2}{\alpha_l}. \end{aligned} \tag{6.49}$$

$\square$

## Acknowledgments

This work has been partially supported by the National Science Foundation under grant number DMS-9971209. The author wishes to thank Professor Steven Cox and Professor Chrysoula Tsogka for helpful discussion and encouragement. The author is also grateful for the very useful suggestions made by the referees.

## References

- [1] Adams R A 1975 *Sobolev Spaces* (New York: Academic)
- [2] Allers A and Santosa F 1991 Stability and resolution analysis of a linearized problem in electrical impedance tomography *Inverse Problems* **7** 515–33
- [3] Berryman J G and Kohn R V 1990 Variational constraints for electrical impedance tomography *Phys. Rev. Lett.* **65** 325–8
- [4] Brandt A 1984 Multigrid techniques: 1984 guide with applications to fluid dynamics *Gesellschaft für Mathematik und Datenverarbeitung* (Bonn: MBH)
- [5] Brandt A 1977 Multi-level adaptive solutions to boundary-value problems *Math. Comput.* **31** 333–90
- [6] Brenner S C and Scott L R 1994 *The Mathematical Theory of Finite Elements Methods* (New York: Springer)
- [7] Brown R M and Uhlmann G 1997 Uniqueness in the inverse conductivity problem for nonsmooth conductivities in two dimensions *Commun. Pure Appl. Math.* **22** 1009–27
- [8] Calderón A P 1980 On an inverse boundary value problem *Seminar on Numerical Analysis and its Applications to Continuum Physics* (Rio de Janeiro: Soc. Brasileira de Matemática) pp 65–73
- [9] Cheney M, Isaacson D, Newell J C, Goble J and Simske S 1990 NOSER: an algorithm for solving the inverse conductivity problem *Int. J. Imaging Syst. Technol.* **2** 66–75
- [10] Cheney M, Isaacson D and Newell J C 1999 Electrical impedance tomography *SIAM Rev.* **41** 85–101
- [11] Colton D and Kress R 1998 *Inverse Acoustic and Electromagnetic Scattering Theory* 2nd edn (Berlin: Springer)
- [12] Curtis E B and Morrow J A 1990 Determining the resistors in a network *SIAM J. Appl. Math.* **50** 931–41
- [13] Dennis J E and Schnabel R B 1996 *Numerical Methods for Unconstrained Optimization and Nonlinear Equations* (Philadelphia, PA: SIAM)
- [14] Dobson D C 1992 Convergence of a reconstruction method for the inverse conductivity problem *SIAM J. Appl. Math.* **52** 442–58
- [15] Dobson D C and Santosa F 1994 Resolution and stability analysis of an inverse problem in electrical impedance tomography: dependence on the input current patterns *SIAM J. Appl. Math.* **54** 1542–60
- [16] Dorn O, Bertete-Agiurre H, Berryman J G and Papanicolaou G C 1999 A nonlinear inversion method for 3D-electromagnetic imaging using adjoint fields *Inverse Problems* **15** 1523–58
- [17] Druskin V 1982 The unique solution of the inverse problem of electrical surveying and electrical well-logging for piecewise-continuous conductivity *Izv. Earth Phys.* **18** 51–3
- [18] Engl H 1993 Regularization methods for the stable solution of inverse problems *Surv. Math. Ind.* **3** 71–143
- [19] Folland G B 1995 *Introduction to Partial Differential Equations* (Princeton, NJ: Princeton University Press)
- [20] Francini E 2000 Recovering a complex coefficient in a planar domain from the Dirichlet to Neumann map *Inverse Problems* **16** 107–19
- [21] Fucks L F, Cheney M, Isaacson D, Gisser D G and Newell J C 1991 Detection and imaging of electric conductivity and permittivity at low frequency *IEEE Trans. Biomed. Eng.* **38** 1106–10
- [22] Garbow B S, Hillstom K E and Moré J J 1980 *Minpack Project, Argonne National Laboratory* Minpack and subroutine hybrj are available in NETLIB at webpage <http://www.netlib.org/minpack/>
- [23] Gill P E, Murray W and Wright M H 1989 *Practical Optimization* 8th edn (London: Academic)
- [24] Hackbusch W 1985 *Multi-Grid Methods and Applications* (Berlin: Springer)
- [25] Han Q and Lin F 1997 *Elliptic Partial Differential Equations (Courant Lecture Notes in Mathematics)* (Courant Institute of Mathematical Sciences, New York University, New York)
- [26] Isakov V 1998 *Inverse Problems for Partial Differential Equations* (New York: Springer)
- [27] Johnson C 1992 *Numerical Solution of Partial Differential Equations by the Finite Element Method* (Cambridge: Cambridge University Press)
- [28] Kaipio J P, Kolehmainen V, Somersalo E and Vauhkonen M Statistical inversion methods in electrical impedance tomography *Preprint*
- [29] Kohn R V and McKenney A 1990 Numerical implementation of a variational method for electrical impedance tomography *Inverse Problems* **6** 389–414

- [30] Kohn R and Vogelius M 1984 Determining conductivity by boundary measurements *Commun. Pure Appl. Math.* **37** 113–23
- [31] Ladyzhenskaya O A and Ural'tseva N N 1968 *Linear and Quasilinear Elliptic Equations* (New York: Academic)
- [32] Lieb E H and Loss M 1997 *Analysis, Graduate Studies in Mathematics* vol 14 (Providence, RI: American Mathematical Society)
- [33] McCormick S F and Wade J G 1993 Multigrid solution of a linearized, regularized least-squares problem in electrical impedance tomography *Inverse Problems* **9** 697–713
- [34] Nachman A I 1996 Global uniqueness for a two-dimensional inverse boundary problem *Ann. Math.* **143** 71–96
- [35] Natterer F 1995 Numerical solution of bilinear inverse problems *Preprint*
- [36] Ortega J M and Rheinboldt W C 1970 *Iterative Solution of Nonlinear Equations in Several Variables* (San Diego, CA: Academic)
- [37] Ramirez A, Daily W, LaBrecque D, Owen E and Chestnut D 1993 Monitoring an underground steam injection process using electrical resistance tomography *Water Resour. Res.* **29** 73–87
- [38] Ramirez A, Daily W, Binley A, LaBrecque D and Roelant D 1996 Detection of leaks in underground storage tanks using electrical resistance methods *J. Environ. Eng. Geophys.* **1** 189–203
- [39] Santosa F, Vogelius M and Xu Jiang-Ming 1998 An effective nonlinear boundary condition for a corroding surface. Identification of the damage based on steady state electric data *Z. Angew. Math. Phys.* **49** 656–79
- [40] Siltanen S, Mueller J and Isaacson D 2000 An implementation of the reconstruction algorithm of A Nachman for the 2-D inverse conductivity problem *Inverse Problems* **16** 681–99
- [41] Somersalo E, Cheney M, Isaacson D and Isaacson E L 1991 Layer-stripping: a direct numerical method for impedance imaging *Inverse Problems* **7** 899–926
- [42] Strikwerda J C 1989 *Finite Difference Schemes and Partial Differential Equations* (Pacific Grove, CA: Wadsworth and Brooks–Cole)
- [43] Sylvester J 1992 A convergent layer stripping algorithm for radially symmetric impedance tomography problem *Commun. Partial Diff. Eq.* **17** 1955–94
- [44] Sylvester J and Uhlmann G 1987 A global uniqueness theorem for an inverse boundary value problem *Ann. Math.* **125** 153–69
- [45] Wexler A, Fry B and Neuman M 1985 Impedance-computed tomography algorithm and system *Appl. Opt.* **24** 3985–92
- [46] Yorkey T J, Webster J G and Tompkins W J 1987 Comparing reconstruction algorithms for electrical impedance tomography *IEEE Trans. Biomed. Eng.* **34** 843–52
- [47] Zhang J 1999 Acceleration and stabilization properties of minimal residual smoothing technique in multigrid *Appl. Math. Comput.* **100** 151–68
- [48] Zhang J 1998 Multi-level minimal residual smoothing: a family of general purpose multigrid acceleration techniques *J. Comput. Appl. Math.* **100** 41–51